Loss of HDAC11 accelerates skeletal muscle regeneration

Journal:	*The FEBS Journal*
Manuscript ID	FJ-20-0355.R1
Manuscript Type:	Regular Paper
Date Submitted by the Author:	n/a
Complete List of Authors:	Suelves, Monica; Foundation Institute of Research in Health Sciences Germans Trias i Pujol, PMPPC Núñez-Álvarez, Yaiza; Foundation Institute of Research in Health Sciences Germans Trias i Pujol, PMPPC Hurtado, Erica; Foundation Institute of Research in Health Sciences Germans Trias i Pujol, PMPPC Muñoz, Mar; Foundation Institute of Research in Health Sciences Germans Trias i Pujol, PMPPC García-Tuñon, Ignacio; Institute of Molecular and Cellular Biology of Cancer Rech, Gabriel; Foundation Institute of Research in Health Sciences Germans Trias i Pujol Pluvinet, Raquel; Foundation Institute of Research in Health Sciences Germans Trias i Pujol Sumoy, Lauro; Foundation Institute of Research in Health Sciences Germans Trias i Pujol Pendas, Alberto; Institute of Molecular and Cellular Biology of Cancer Peinado, Miguel; Foundation Institute of Research in Health Sciences Germans Trias i Pujol, PMPPC
Key Words:	

Loss of HDAC11 accelerates skeletal muscle regeneration

Yaiza Núñez-Álvarez[1]*[+], Erica Hurtado[1]*, Mar Muñoz[1], Ignacio García-Tuñon[2], Gabriel E. Rech[1++], Raquel Pluvinet[1], Lauro Sumoy[1], Alberto M. Pendás[2], Miguel Ángel Peinado[1] and Mònica Suelves[1]**

* Equal contribution

[1]Germans Trias i Pujol Health Sciences Research Institute (IGTP), Can Ruti Campus, Badalona, Spain.
[2] Institute of Cellular and Molecular Biology of Cancer (CSIC-USAL), Salamanca, Spain.

Yaiza Núñez-Álvarez: yaiza.nunez-alvarez@igh.cnrs.fr

Erica Hurtado: ehurtado@igtp.cat

Mar Muñoz: mmunoz@igtp.cat

Ignacio García-Tuñon: ignacio.tunon@usal.es

Gabriel E. Rech: gabriel.rech@ibe.upf-csic.es

Raquel Pluvinet: rpluvinet@igtp.cat

Lauro Sumoy: lsumoy@igtp.cat

Alberto M. Pendás: amp@usal.es

Miguel A. Peinado: mpeinado@igtp.cat

Mònica Suelves: msuelves@igtp.cat

+Present address: Institute of Human Genetics, IGH-UMR9002 CNRS/UM, 34396 Montpellier Cedex 5, France

++Present address: Institute of Evolutionary Biology, CSIC- UPF, Barcelona, Spain

** Correspondence to:

Mònica Suelves

Germans Trias i Pujol Research Institute (IGTP), Program of Predictive and Personalized Medicine of Cancer, Can Ruti Campus, Crta de Can Ruti, Camí de les Escoles s/n, 08916 Badalona, Spain

Phone: 34 935543058

E-mail: msuelves@igtp.cat

Running title: HDAC11 deficiency advances skeletal muscle regeneration

Keywords: HDAC11, skeletal muscle regeneration, muscle differentiation, satellite cells, cell cycle exit, macrophages, IL-10

Abbreviations: bp, base pairs; BrdU, bromodeoxyuridine; ChIP, chromatin immunoprecipitation; CNF, central-nucleated fiber, CpGi, CpG island; CSA, cross-sectional area; CTX, cardiotoxin; DAPI, 4',6-diamino-2-phenylindole; DM, differentiation medium; dpi, days post injury; eMYHC, embryonal myosin heavy chain; FACS, fluorescence-activated cell sorting; FBS, foetal bovine serum; GC, gastrocnemius; GM, growth medium; HDAC11, histone deacetlyase 11; H/E, hematoxylin and eosin; HS, horse serum; HRP, horseradish peroxidase; IL-1β; Interleukin 1 beta; IL-10, Interleukin 10; KO, knockout; M1, macrophages type 1; M2, macrophages type 2; MPCs, muscle precursor cells; PAX7 paired-box transcription factor 7; RT-qPCR, reverse transcription quantitative polymerase chain reaction; SL, soleus; SCs, satellite cells; SD, standard deviation; shRNA, short-hairpin RNA; TA, tibialis anterior; TNFα, tumour necrosis factor alpha; TSS, transcription start site; WB, Western Blot; WT, wild type.

Abstract

HDAC11 is the latest identified member of the histone deacetylase family of enzymes. It is highly expressed in brain, heart, testis, kidney and skeletal muscle, although its role in these tissues is poorly understood. Here we investigate for the first time the consequences of HDAC11 genetic impairment in skeletal muscle regeneration, a process principally dependent on its resident stem cells (satellite cells) in coordination with infiltrating immune cells and stromal cells. Our results show that HDAC11 is dispensable for adult muscle growth and establishment of the satellite cell population, while HDAC11 deficiency advances the regeneration process in response to muscle injury. This effect is not caused by differences in satellite cell activation or proliferation upon injury, but rather by an enhanced capacity of satellite cells to differentiate at early regeneration stages in the absence of HDAC11. Infiltrating HDAC11-deficient macrophages could also contribute to this accelerated muscle regenerative process by prematurely producing high levels of IL-10, a cytokine known to promote myoblast differentiation. Altogether, our results show that HDAC11 depletion advances skeletal muscle regeneration and this finding may have potential implications for designing new strategies for muscle pathologies coursing with chronic damage.

Introduction

Skeletal muscle, the largest tissue in mammalian organisms, has an extraordinary capacity to regenerate after injury thanks to its resident stem cells, called satellite cells, which are located between the sarcolemma and the basal lamina [1]. Satellite cells are in quiescence (a G0 reversible arrest state) in resting muscle and are characterized by the expression of the paired-box transcription factor PAX7 [2]. In response to stimuli, such as injury or disease, satellite cells activate and proliferate to give rise to proliferating myoblasts, who exit the cell cycle before differentiating and fusing to form multinucleated myotubes and restore the damaged tissue. Alternatively, after cell cycle exit, a small subpopulation of myoblasts undergoes self-renewal to restore the reserve population of quiescent satellite cells [3]. Re-establishment of this quiescent stem cell population and growth and maturation of the newly formed myofibers are signs of muscle homeostasis recovery.

The efficiency of the skeletal muscle regeneration process also requires the coordinated action of satellite cells and inflammatory cells [4]. Following an acute injury, muscle is infiltrated by neutrophils, followed by monocyte-derived macrophages that acquire a pro-inflammatory phenotype representing the “classical activated” M1 macrophage population. M1 macrophages phagocytose necrotic muscle debris and secrete large amounts of pro-inflammatory cytokines such as IL-6, TNFα and IL-1β, which promote myoblast proliferation while repressing differentiation [5]. Subsequently, a distinct “pro-regenerative” macrophage population with anti-inflammatory phenotype (named “alternatively activated” M2 macrophages) becomes more prevalent, and suppresses the process of inflammation while supporting restorative functions. This bipolar classification in M1 and M2 macrophages represents the polarized

extremes of a range of macrophage phenotypes that coexist in a continuum of activation states and, despite its simplicity, it is widely used to facilitate the understanding of macrophage functions. In regenerating skeletal muscles, a marked increase of anti-inflammatory cytokines such as IL-10 coincides with the M1 to M2 macrophage transition, which in turn regulates the transition of satellite cells from their proliferative to differentiation state to facilitate regeneration [4].

Histone deacetylases (HDACs) regulate many biological functions by removing acetyl groups from lysine ε -amino groups on histone and non-histone proteins. In mammals there are 18 HDAC proteins divided in two families, the Zn^{2+} dependent or classical HDACs (subclassified in class I, II and IV) and the nicotinamide adenine dinucleotide (NAD+) dependent HDACs (class III HDACs) named sirtuins [6]. HDAC11 is the only member of the class IV HDAC subfamily and the latest member identified [7,8] and remains still one of the less studied HDACs. Since its discovery 18 years ago, its expression is known to be enriched in skeletal muscle, however its role in myogenesis remains practically uninvestigated. Here, we aim to address for the first time the role of HDAC11 in skeletal muscle regeneration. To address this, we studied the physiological consequences of the genetic loss of HDAC11 during the *in vivo* process of myogenesis, by inducing acute muscle injury in HDAC11 knockout mice and analysing its regeneration capacity. Our results show that loss of HDAC11 accelerates skeletal muscle regeneration, by acting on specific satellite cell functions and macrophage cytokine production that enhance satellite cell differentiation, providing a new role for HDAC11.

Results

HDAC11 is the HDAC member with maximal gene-expression induction at the onset of satellite-cell differentiation

HDAC11 is highly expressed in skeletal muscle [7] but its role in myogenesis remains poorly understood. Using our previous transcriptomic datasets of satellite-cell-derived primary myoblasts in proliferation and differentiation conditions [9], we observed that HDAC11 was the HDAC member whose expression changes the most at the transition from proliferating myoblasts (P) to differentiating myocytes (day 1 of differentiation, D1) (Figure 1A). To validate this result, we analysed by RT-qPCR the expression level of all classical HDACs in four independent sets of satellite cell-derived primary myoblasts in proliferation and 1 day in differentiation conditions. As shown in Figure 1B, among all HDACs, the most expressed were HDAC1 and HDAC3, both members of class I HDACs, and their expression did not change under differentiation conditions. HDAC2 was not detected at any point and HDAC8 expression levels remained very low and unchanged. Among class II HDAC members, HDAC4, HDAC5, HDAC6 and HDAC10 maintained similar expression levels in both proliferation and differentiation conditions, while HDAC9 was upregulated (3.8 folds) and HDAC7 down-regulated (to almost half of its expression) upon differentiation, as reported [10,11]. Finally, and in agreement with our transcriptomic data, HDAC11 showed the maximal up-regulation (4.5 fold) 1 day after differentiation, being this induction detected as early as 12 h in differentiation conditions (Figure 1C). Notably, HDAC11 expression upregulation was also confirmed in human primary myoblasts and in C2C12 myoblast cell line at the onset of muscle differentiation (Supplemental Figure 1 and Figure 1C, respectively).

Next, we investigated the mechanisms regulating HDAC11 expression during muscle differentiation, focussing in particular on its epigenetic control. HDAC11 contains a CpG island (CpGi) on its promoter region; we therefore analysed the DNA methylation level of CpG dinucleotides at CpGi and shore regions by bisulfite conversion in three independent cultured mouse satellite-cell-derived primary myoblasts. As shown in Supplemental Figure 2A, all analysed CpGs were totally unmethylated in proliferating and differentiated primary muscle cells, indicating that HDAC11 expression is not epigenetically regulated by DNA methylation in proliferating conditions. Thanks to available ENCODE data [12], we compared the histone marks profile of the HDAC11 locus in proliferating and differentiating C2C12 myoblast cells. The histone marks positively associated with gene expression, H3K4me3 and H3ac, were already present around the transcription start site in proliferating and differentiated myoblast cells, with H3K4me3 levels increasing in differentiating cells, while H3ac levels were very similar in both cellular states (Supplemental Figure 2B). Of note, marks deposited as a consequence of transcriptional elongation, H3K79me2 and H3K36me3, were absent in proliferating cells and increased in differentiating cells, correlating with the induction of gene expression, whereas the levels of H3K27me3, the polycomb repressive mark associated with repressed chromatin, were almost negligible in both states (Supplemental Figure 2B). This epigenetic landscape indicated that the increase of HDAC11 mRNA levels in differentiating muscle cells is due to increased gene transcription (evidenced by the increase of H3K4me3, H3K79me2 and H3K36me3 marks). However, the presence of permissive chromatin marks and the absence of repressive ones, both in proliferating and differentiating conditions, suggests that HDAC11 silencing in proliferating cells is neither mediated by epigenetic polycomb repression nor DNA methylation. To assess whether HDAC11 induction in

differentiating cells was triggered by myogenic transcription factor binding, we analysed the MYOD and myogenin (MYOG) ChIP-Seq ENCODE data in proliferating and differentiating C2C12 cells [12]. As shown in Figure 1D, MYOD was bound to the HDAC11 promoter region at day 1 (D1) and day D2.5 of differentiation but not in proliferation conditions. Further on, MYOG was found to bind HDAC11 promoter at D1, increasing its association thereafter (D2.5) (Figure 1D). It is well known that MYOD and MYOG form heterodimers with E-proteins of the bHLH subfamily, such as E12/E47 (TCF3) and HEB (TCF12), to bind DNA [13]. Notably, ChIP-seq data of TCF3 and TCF12 in C2C12 differentiating cells also showed their binding at the same region of the HDAC11 proximal promoter (Figure 1D). Altogether, these results would suggest HDAC11 as a new target of MYOD and MYOG transcription factors, which highly induce its expression at the onset of skeletal muscle differentiation.

HDAC11 is dispensable for adult skeletal muscle growth and homeostasis

To study the biological function of HDAC11 *in vivo*, we generated HDAC11 total knockout mice (HDAC11$^{-/-}$ or KO mice) by a targeted depletion of floxed exon 3 of the *Hdac11* gene [Hurtado et al, *in press*]. The correct genotyping of wild type (WT) and KO mice was assessed by PCR (Supplemental Figure 3A) and by immunoblotting we confirmed the absence of HDAC11 protein in KO mice (Supplemental Figure 3B). HDAC11$^{-/-}$ mice were viable and indistinguishable from WT counterparts, and skeletal muscles showed no overt differences, based on the similar appearance and weight of tibialis anterior (TA) and gastrocnemius (GC) muscles from adult male and female WT and KO mice (Figure 2A). To more deeply assess the consequences of HDAC11 deficiency on the skeletal musculature, we performed histological analysis in TA and GC muscles of both genders. As shown in Figure 2B, HDAC11-deficient

mice did not show any obvious alteration in skeletal muscle architecture, neither differences in the number of myofibers per muscle area nor cross-sectional area (CSA). Furthermore, HDAC11$^{-/-}$ and WT muscles showed very similar numbers of PAX7-expressing satellite cells (Figure 2C), which were negative for KI67 immunostaining (data not shown), confirming their quiescent status. These results show that HDAC11 is not essential for normal development and growth of skeletal muscles, neither for the establishment and maintenance of the quiescent satellite cell pool in adult resting muscle.

HDAC11 deficiency accelerates skeletal muscle regeneration

Next, we comparatively analysed the regenerative potential of HDAC11-deficient muscles in response to intramuscular injection of cardiotoxin (CTX), a well-established model of acute muscle injury [14,15] at 4, 7, 21 and 60 days post injury (dpi). Sections of injured TA and GC muscles from WT and HDAC11$^{-/-}$ mice were subjected to hematoxylin and eosin (H/E) staining. At day 4 post injury, both WT and HDAC11$^{-/-}$ TA muscles showed numerous mononucleated cells (likely proliferating myoblasts and inflammatory infiltrating cells) and early regenerating myotubes, with centrally located myonuclei (CNF, central nucleated fibers) (Figure 3A), which express specifically the embryonic/developmental myosin heavy chain isoform (eMYHC) (Figure 3B). At this early regeneration time-point, the average size of newly-forming regenerating myofibers was slightly higher in HDAC11$^{-/-}$ than WT, although this difference was not statistically significant. Myofiber size distribution confirmed the higher proportion of larger myofibers in HDAC11-deficient compared to WT muscles (Figure 3A). At the more advanced regeneration time point of 7 days after injury, the size of regenerating myofibers with centrally-located myonuclei (CNF) increased in both mouse genotypes;

however the average of eMYHC+ myofiber size was significantly higher in HDAC11-/- compared to WT mice, and this was true for both TA and GC muscles (Figure 3A-B and Supplemental Figure 4A). The distribution of regenerating myofibers by size confirmed a reduced number of smaller fibers and higher number of larger fibers in HDAC11-deficient muscles of male mice (Figure 3A-B and Supplemental Figure 4A). Similar results were observed in female mice, with increased average mean area of eMYHC+ regenerating myofibers and higher percentage of larger myofibers at 7 dpi the in HDAC11-deficient muscles (Supplemental Figures 4B-C). Of note, after completion of the regeneration process, myofibers of both genotypes continued to grow and mature, reaching a similar final size 21 and 60 days after damage (Figure 3A). Together, these results indicate that HDAC11 plays a role during early myofiber formation and growth following damage, but is dispensable for the final myofiber maturation phase leading to homeostasis.

HDAC11 deficiency alters satellite-cell differentiation kinetics during skeletal muscle regeneration

We next examined the underpinning of the advanced muscle regeneration process in the absence of HDAC11. We observed no differences in the number of early-activated satellite cells (MYOD+/PAX7+ cells) at 6 hours (not shown) or proliferating satellite cells (KI67+/PAX7+ cells) at 4 days (Supplemental Figure 5A) after injury, suggesting that HDAC11 depletion does not alter satellite cell activation and proliferation early after injury. At 4dpi, HDAC11-/- muscles did not show any differences in the number of differentiating myocytes (MYOG+ cells) compared to WT (Supplemental Figure 5B). In contrast, at 7 dpi, the total number of PAX7+ cells was significantly reduced in KO muscles, correlating with a significant

increase of differentiating MYOG+ cells (Figure 4A). Interestingly, the number of proliferating cells (KI67+/PAX7+ cells) within the overall PAX7-expressing satellite-cell population was higher in HDAC11-/- muscles (Figure 4A), and this feature was maintained at 21 dpi, indicating a sustained satellite cell-proliferative state in the absence of HDAC11 (Figure 4B). When muscles reached full maturation and homeostasis (i.e. 60 dpi), muscle from both mouse genotypes showed the same number of PAX7+ cells per 100 fibers, being all of them negative for the proliferation marker KI67, indicating a total restoration of the quiescent satellite cell pool (Figure 4C). Collectively, these results suggest that during the regeneration process, HDAC11-deficient satellite cells activate and proliferate normally, but at late stages of the regeneration process, HDAC11-deficient satellite cells differentiate faster (see 7dpi) and take longer to complete the full return to quiescence (see 21dpi).

Satellite cell-intrinsic loss of HDAC11 enhances myogenic differentiation

To investigate the potential cell-autonomous role of HDAC11 in satellite cells during myogenesis, we isolated satellite cells by fluorescent-activated cell sorting (FACS) from WT and KO mice (Supplemental Figure 6A) and analysed their ability to proliferate and differentiate *in vitro*. Equal numbers of freshly isolated WT and HDAC11-/- satellite cells were plated, and number of cells was counted after 24, 48 and 72 hours of culture in proliferation medium (GM). The satellite-cell growth curves and the number of cells incorporating bromodeoxyuridine (BrdU) were similar in both genotypes (Figure 5A and Supplemental 6B). These results confirm that HDAC11 deficiency does not alter the proliferation capacity of satellite cells.

Next, we evaluated the differentiation and fusion capacities of HDAC11$^{-/-}$ satellite cells in differentiation medium (DM) for 24 and 72 hours, by MYOG and eMYHC staining, respectively. As shown in Figure 5B, the number of MYOG^{+} cells over total cell number was significant higher in HDAC11-deficient cells at the early differentiation time-point of 24 h DM (Figure 5B). At 72h in DM, however, almost 100% of both WT and KO cells were positive for eMYHC, and the fusion index, calculated by counting the number of myonuclei in eMYHC^{+} myotubes over total number of nuclei, did not show significant differences between genotypes (Figure 5C). Consistent with this, the expression levels of classical fusion regulators, such as myomaker, or myomixer did not change in differentiating HDAC11-deficient cells, and only the expression of dysferlin (a plasma membrane protein involved in myofiber repair) was significantly higher in HDAC11-deficient myotubes (Figure 5C). These results would indicate that loss of HDAC11 accelerates the differentiation capacity of satellite cells but does not promote their fusion.

HDAC11$^{-/-}$ myoblasts express higher levels of cell cycle-related genes and exhibit sustained proliferation in differentiating conditions

To get further insight into the molecular changes caused by HDAC11 loss at early myogenic differentiation, we performed RNA sequencing (RNA-seq) from FACS isolated satellite cell-derived primary myoblasts from WT and HDAC11-deficient mice, and further differentiated in DM for 24 hours (data deposited in NCBI's Gene Expression Omnibus accessible through GEO Series accession number GSE147423). A total of 416 genes were up-regulated whereas 213 genes were down-regulated in HDAC11$^{-/-}$ differentiating myoblasts versus the WT counterparts (p adj val <0,05 and FC >2 in absolute value). Interestingly, Gene Ontology (GO)

analysis revealed a statistically significant enrichment of genes involved in cell cycle regulation (Figure 6A and Supplemental Table 6), consistent with the sustained *in vivo* proliferation observed during skeletal muscle regeneration. To validate the RNA-seq results, we generated HDAC11 shRNA (sh28-HDAC11) and control shRNA (shCtrl) C2C12-myoblast stable cell lines and, as shown in Figure 6B, HDAC11 mRNA was effectively down-regulated in sh28-HDAC11 C2C12 cells compared to control cells, upon 24 hours in DM. Next, we analysed the expression level of cell-cycle related genes including AurkA, AurkB, Ki67, and Pcna and confirmed that all of them were significantly up-regulated upon HDAC11 knockdown in differentiating conditions (Figure 6B), thus validating the RNA-seq results and supporting sustained proliferation of myoblasts when HDAC11 is ablated.

Down-regulated genes in HDAC11-deficient cells at day 1 of differentiation were related to "muscle system process" and "muscle contraction" GO categories, including several sarcomeric- and calcium sensing/releasing-related genes (Figure 6A and Supplemental Table 7). However, no changes in the expression of these genes were found *in vivo*. In fact, similar expression levels of sarcomeric cytoskeleton genes such as myomesin 2 and 3 (Myom1, 2), titin (Ttn), and actinin alpha 3 (Actn3), and calcium sensing/releasing-related genes such as triadin (Trdn), tropomodulin (Tmod) and ryanodine receptor 1 (Ryr1) were observed in TA muscles from WT and HDAC11-deficient mice (Figure 6C), suggesting that genetic impairment of HDAC11 does not compromise the overall expression of structural contractile proteins in adult skeletal muscles.

As RNA-seq data showed alterations in cell cycle-exit genes, we cultured WT and HDAC11-deficient myoblasts in DM (which contains low serum) to allow cell-cycle withdrawal. We

analysed the proportion of replicating cells, by quantifying the number of cells that incorporate 5-ethynyl-2'-deoxyuridine (EdU) at 3, 6, 24 and 36 hours of differentiation. As shown in Figure 6D, 6 hours after the switch to low-serum medium HDAC11-deficient myoblasts showed 18% more cells remaining in S phase compared to WT, and this difference was significantly higher at 12 and 24 hours of differentiation (33% and 62%, respectively), supporting the notion that HDAC11-deficient myoblasts show a reduced ability to exit the cell-cycle under cell-cycle withdrawal-differentiating conditions (Figure 6D).

Histone deacetylases can remove acetyl groups from lysines residues in histone proteins increasing gene transcription [6]. To address if higher acetylation levels in promoter regions could explain the higher expression of cell cycle related genes in HDAC11-deficient cells, we performed chromatin immunoprecipitation (ChIP) assays. We compared H3 total acetylation levels (panH3ac) and the specific acetylation in H3K9 (H3K9ac) in C2C12 cells with specific HDAC11 targeting shRNAs (shRNA24-HDAC11 and shRNA28-HDAC11) and control cells (shCtrl-C2C12), at 24 hours in DM. As shown in Figure 6E and Supplemental Figure 7, the expression level of the genes analysed (Aurka, Aurkb and Pcna) was significantly higher in shRNA-HDAC11 cells, but the level of acetylation marks in the corresponding promoter regions did not show differences between samples. These results suggest that the up-regulation of cell cycle related genes in HDAC11-deficient muscle cells, which account for their sustained proliferation, is not mediated by increased H3 acetylation levels due to the reduction of HDAC11 histone deacetylase activity.

HDAC11-deficient macrophages overexpress IL-10

Following muscle injury, infiltrating macrophages play a critical role during the skeletal muscle regeneration process [16]. Macrophages are required not only for the clearance of necrotic debris at early stages of regeneration, but also at late stages for promoting muscle differentiation [17,18]. As HDAC11 is highly expressed in immune cells [19–21], we examine the infiltrating macrophages of HDAC11-deficient mice at 4 and 7 post-CTX injury. FACS analysis did not show differences in the relative distribution of macrophage pro-inflammatory (M1) and anti-inflammatory/pro-regenerative (M2) subpopulations in muscles of both genotypes at 4 and 7 days post injury (Figure 7A-B). However, analysis of the expression level of various cytokines produced by M1 and M2 macrophages showed variations between WT and HDAC11-deficient cells. At 4 days after CTX injection, we found a mixed pro- and anti-inflammatory phenotype of HDAC11-deficient macrophages; M1 macrophages expressed higher levels of IL-6 and IL-1β cytokines (Figure 7C), whereas M2 macrophages expressed higher levels of the anti-inflammatory cytokine IL-10, the main target for HDAC11 known so far [19] (Figure 7D). At 7dpi, the number of M1 macrophages was extremely low, as expected, impeding cytokine expression analysis; the expression of anti-inflammatory cytokines in M2 macrophages at this late time-point showed no differences between WT and KO cells (Figure 7D). These results indicate that the absence of HDAC11 does not impact on macrophage infiltration upon muscle injury, neither the ratio between M1/M2 macrophage populations at 4 nor 7 dpi. However, loss of HDAC11 results in increased levels of IL-10, suggesting a faster transition towards an anti-inflammatory/pro-regeneration environment, which would result in a more efficient regeneration of HDAC11-deficient muscle.

Discussion

Our study evaluates for the first time the consequences of HDAC11 deficiency in skeletal muscle regeneration. Skeletal muscle is able to undergo extensive regeneration thanks to the capacity of its resident quiescent stem cells (named satellite cells) to activate, proliferate and differentiate in response to muscle injury. These satellite cell activities occur in coordination with sequential waves of pro-inflammatory and anti-inflammatory macrophages, whose signals affect satellite cell behaviour [5]. Our results showed that loss of HDAC11 accelerates skeletal muscle regeneration. This effect cannot be attributed to HDAC11 effects on satellite cell activation or proliferation, rather on the enhanced differentiation capacity of satellite cells lacking HDAC11. Because the anti-inflammatory cytokine IL-10 promotes myoblast differentiation and exerts a pro-recovery action in injured muscle [17,22] it is tempting to propose that the prematurely high levels of this cytokine in HDAC11-deficient macrophages also contribute to propel muscle regeneration.

In mammals there are 18 HDACs proteins subclassified in class I (HDAC1, HDAC2, HDAC3 and HDAC8), class II (HDAC4, HDAC5, HDAC6, HDAC7, HDAC9 and HDAC10), class III (SIRT 1-7) and class IV (HDAC11) [6]. By comparing HDACs expression between proliferation and the early onset of muscle differentiation, when key transcriptional changes to induce cell cycle exit and initiate the differentiation gene program occur, we find that only the expression of HDAC7, HDAC9 and HDAC11 changes at this transition. HDAC7 and HDAC9 belong to the class IIa HDACs, which represses MEF2 dependent transcription during myoblasts proliferation [10,23–25]. At present, HDAC11 is the unique member of class IV

HDACs due to differences in its catalytic core region compared with the rest of HDACs [7,8]. Notably, we show that is the most upregulated HDAC at the early onset of muscle differentiation.

The induction of HDAC11 expression has also been reported in cardiomyocyte differentiation [26,27], oligodendrocyte differentiation [28] and post-natal neuron formation [29], although its target genes/proteins remain uncharacterized. In addition, fibroblasts arrested by serum deprivation or high density conditions also induced HDAC11 expression [30]; and during the neuronal differentiation process HDAC11 and KI67 proteins rarely colocalize in the same cell [28]. These observations are consistent with our data, which show very low expression of HDAC11 in proliferating myoblasts and a fast and high induction when myoblasts exit cell cycle to differentiate prior to forming myotubes. Our RNA-seq data showed a global up-regulation of genes related to mitotic cell cycle and regulation of cell cycle progression in myocytes deficient for HDAC11 at the early stages of differentiation, which is in agreement with the higher proportion of replicating myoblasts under cell-cycle withdrawal conditions, suggesting that HDAC11 induction is required for efficient induction of cell cycle exit. Interestingly, it has been reported that HDAC11 can bind and reversible deacetylate the replication licensing factor Cdt1 (a key factor in the assembly of pre-replication complexes during cell division), which can be ubiquitylated and subsequent degraded by the proteasome upon deacetylation [31]. In addition, the HDAC11 interactome performed assessed in T cells identified members of cohesin complex as prominent HDAC11 interactors [32].

Not all HDACs regulate the expression of their substrate genes equally in the same manner. Class I HDACs show a very high deacetylase activity in contrast to the minimal catalytic

activity detected in class II HDACs, which recruit members of class I on specific target genes to remove the acetyl groups in promoter gene regions [33]. HDAC11 has, as class II HDACs, a very poor activity against acetylated substrates and, very recently it has been demonstrated that HDAC11 has a very potent defatty-acylase activity compared to its minor deacetylase activity on histone and non-histone proteins [34,35]. Thus, it was not surprising that the increased expression levels of cell-cycle related genes in HDAC11-deficient myoblasts did not involve increased acetylation levels of their corresponding promoter regions. Future experiments should address how HDAC11 regulates its substrates in skeletal muscle cells.

Our study suggests that HDAC11 is a new MYOD/MYOG target gene at the onset of skeletal muscle differentiation. The analysis of the chromatin landscape of the *Hdac11* locus showed absence of DNA methylation and polycomb repressive mark (H3K27me3), both in proliferation and differentiation conditions, while histone marks deposited as a consequence of gene transcription (H3K4me3, H3K36me3 and H3K79me2) increased in differentiating cells. Interestingly, public ChIP-seq data of MYOD, MYOG and their coactivators E12/E47 (TCF3) and HEB (TCF12) showed binding of all these transcription factors to HDAC11 proximal promoter only in differentiating cells. In addition, a ChIP-on-chip experiments revealed that MYOD and MYOG were exclusively bound to HDAC11 promoter in differentiated myotubes [36]. Moreover, the depletion of BAF60C, which facilitates MYOD transcription, caused a 4 fold reduction of HDAC11 expression in differentiating C2C12 cells compared to the scrambled control [37], and depletion of functional MYOD or MYOG proteins in primary differentiating myoblasts also resulted in reduced expression of HDAC11 [38,39].

Several classical HDACs contribute to tissue development, and total knock-out mice for HDAC1, HDAC3, HDAC4, HDAC7 and HDAC8 are embryonal or perinatal lethal indicating that they are essential for cell differentiation and tissue development [40]. To our knowledge, total knockout mice for HDAC10 have not been generated yet and, at present, the total knockout mouse model for HDAC6 is the only one with no obvious phenotype [41]. Our results show that HDAC11 total knockout mice are viable and fertile and do not present skeletal muscle alterations in terms of number and size of myofibers or satellite cell number in adulthood. These results indicate that HDAC11 is dispensable for life, for skeletal muscle development and growth, and for the establishment and maintenance of the adult quiescent satellite cell pool.

Contrasting with the dispensability of HDAC11 for muscle homeostasis, HDAC11-deficient mice showed advanced skeletal muscle regeneration following injury, with enhanced number of differentiating satellite cells. *In vitro* myogenic experiments confirmed higher number of MYOG positive cells at early differentiation stages in the absence of HDAC11, although this did not translate in higher fusion rates. These results seem to be paradoxical respect to the high induction of HDAC11 during muscle differentiation, but in agreement with our data, a recent report showed that overexpression of HDAC11 in C2C12 myoblasts inhibits differentiation by repressing MYOG and MEF2C expression, although no loss-of-function experiments nor *in vivo* genetic analyses were performed in that study [42]. Finally, although the advanced regeneration of HDAC11-deficient mice was normalized at late stages after muscle injury, and muscle homeostasis was equally reached in both genotypes, HDAC11-deficient satellite cells presented sustained proliferation even when their WT counterparts had returned to full

quiescence. This is consistent with the deregulated expression of cell cycle genes observed in the RNA-seq data and the observed delay in cell cycle exit *in vitro* and *in vivo*. Altogether, our results would suggest distinct roles of HDAC11 along the myogenic pathway, regulating the exit of cell cycle and the expression of early-muscle specific genes.

Macrophages can change their phenotype and serve different functions during the process of skeletal muscle regeneration. Unlike M1 pro-inflammatory macrophages, M2 anti-inflammatory macrophages promote the resolution of the regeneration process. Our results show that HDAC11 deficiency does not alter the relative distribution of M1/M2 populations at 4 and 7 days post injury. However, M1 macrophages from HDAC11$^{-/-}$ mice expressed higher levels of pro-inflammatory IL-6 and IL-1β cytokines, whereas M2 macrophages begin to express higher levels of the anti-inflammatory cytokine IL-10 earlier. In human and mouse macrophages it has been reported that HDAC11 is a negative regulator of the anti-inflammatory cytokine IL-10. In fact, IL-10 gene was the first HDAC11 epigenetic target, demonstrating that its expression was repressed by HDAC11-mediated promoter deacetylation [19,43,44]. In addition, it has also been reported that HDAC11 is a negative regulator of the pro-inflammatory IL-1β cytokine [45]. This apparent opposite function of HDAC11 in regulating both cytokines could reflect a tightly regulated control of pro- and anti-inflammatory molecules to prevent uncontrolled inflammation, favouring the return to tissue homeostasis. There are many evidences that macrophages interact with satellite cells thus contributing to tissue repair [46]. Pro-inflammatory cytokines, such as IL-6 and TNFα, secreted by M1 macrophages stimulate satellite cells proliferation. Interestingly, TNFα is a fatty acylated protein that needs to be deacylated by SIRT6 to be secreted [47]. Very recently

it has been reported that HDAC11 can also deacylate TNFα *in vitro* [34], suggesting a potential role of HDAC11 in TNFα signalling. To stop myoblast proliferation and stimulate differentiation, fusion and growth, M2 macrophages release anti-inflammatory factors such as IL-10 and TGFβ [17]. Interestingly, it has been shown that IL-10 is a key signal molecule to induce myogenic differentiation *in vivo* [22], and it has also been demonstrated that higher levels of IL-10 reduce the pathology of mdx muscular dystrophy, increasing muscle differentiation index without affecting satellite cell number [48–50]. In agreement with all these data, our results showing advanced high levels of IL-10 suggest a faster transition towards an anti-inflammatory/pro-regeneration environment, which could result in a more efficient regeneration in HDAC11-deficient mice.

The improvement in skeletal muscle regeneration in the absence of HDAC11 described in this study is in line with beneficial effects observed by reducing HDAC11 in other pathologies. HDAC11 KO mice generated by Dr. E. Seto's laboratory show improved cardiac function upon diabetic cardiac injury, reducing oxidative stress and inflammation [51], are resistant to high-fat diet-induced obesity and metabolic syndrome, enhancing insulin sensitivity and glucose tolerance [52], and displayed amelioration of the paralytic disease symptoms induced by experimental autoimmune encephalomyelitis [53]. HDAC inhibitors are considered promising candidates for treatment of a variety of diseases, including muscular dystrophies. Long treatments with trichostatin A (TSA) and givinostat (both class I and class II HDAC inhibitors) in mdx mice, the mouse model of Duchenne muscular dystrophy (DMD), increased the size of myofibers, reduced fibrotic scars and fatty infiltration and increased whole-body strength [54,55]. Importantly, the beneficial effects of givinostat have recently been

demonstrated in a small group of ambulant DMD patients, which after 1 year of treatment showed a significant reduction in disease progression at histological level [56]. HDACs affect multiple targets and most of current HDAC inhibitors inhibit most of HDAC isoforms. Given the variety of pre-clinical studies showing a beneficial effect of HDAC inhibitor treatments, the development of new and more specific HDAC inhibitors, such as specific HDAC11 inhibitors, could be envisioned as an effective approach to achieve better therapeutic benefits in chronic muscle pathologies, as well as inflammatory and metabolic diseases.

Materials and methods

Animals

HDAC11 total knockout mice (HDAC11$^{-/-}$) were generated as described in [Hurtado et al, *in press*]. HDAC11$^{-/-}$ animals were obtained from undercrossing heterozygote mice and WT littermates were used as controls. To identify the genotype by PCR reaction, primers flanking the deletion region were designed (forward primer: GGAAAGGCACTTTCACTTGC and reverse primer: ACCAACCACACAGCCCATA) and specific amplicon lengths were obtained (1104bp for WT and 181bp for HDAC11$^{-/-}$). Mice were maintained in standard cages under standard conditions: constant temperature (22º±2º), relative humidity (50±10%) and 12-hour light/dark schedule. Standard rodent chow and clean water were available *ad libitum*. WT and HDAC11$^{-/-}$ mice of three months of age were sacrificed by isoflurane inhalation followed by cervical dislocation, in accordance with the ethical approval obtained from the Generalitat de Catalunya (Department of Territory and Sustainability Directorate General for Environmental Policies and Natural Environment, Commission of Animal Experimentation). At least 3 mice of the same sex per group were used in each experiment.

Cell lines

C2C12 cell line was obtained from ATCC, satellite cell-derived mouse primary myoblasts were isolated as described in [57] and satellite cell-derived human primary myoblasts were provided by Dr. Eduard Gallardo (*Hospital de la Santa Creu i Sant Pau,* Autonomous University of Barcelona). Growth medium (GM) and differentiation medium (DM) for C2C12 and satellite cell-derived mouse and human primary myoblasts are detailed in Supplemental Information.

Satellite cells and macrophages isolation by FACS sorting

Isolation of mononucleated satellite cells (SCs) and macrophages cells from heterogeneous populations of muscle extracts were performed as described in [57] and [58], respectively. After isolation, the number of cells was counted in a Neubauer chamber and the cells were frozen in 90% of FBS + 10% DMSO in a cold Mr. Frosty™ and kept in liquid nitrogen until FACS sorting. To perform FACS sorting cells were thawed and centrifuge at 4ºC for 15 minutes at 1.300 rpm and resuspended at $1x10_6$ cell per 100 ul of FACS Buffer (PBS 1X with 2,5% FBS). Cells were incubated for 30 min on ice in darkness with the indicated antibodies against cell surface markers listed in Supplemental Information Table 1. After incubation, cells were washed in FACS buffer, centrifuged at 4ºC for 15 minutes at 1.700 rpm, resuspended in 1 ml of FACS buffer and stained with DAPI to be analysed and sorted. Satellite cells were gated on α7-integrin/CD34 double positive cells. M1 macrophage population was gated on CD11b positive, F4/80 low and Ly6c high staining and M2 macrophage population was gated on CD11b positive, F4/80 high and Ly6c low to negative staining.

Satellite cells and myoblasts proliferation assays

For *ex vivo* proliferation assay, satellite cells isolated by FACs sorting were counted and 70 satellite cells were plated in collagen coated 96 well-plate, and 9 replicates were performed per each cell culture. Satellite cells were grown in GM and at day 1, 2 and 3 after plating, the cells were counted under a microscope. For each genotype (WT and HDAC11$^{-/-}$ cells) at least four independent sets of satellite cells were analysed.

For *in vitro* proliferation assay, satellite cells-derived primary myoblasts were maintained at subconfluent conditions in GM. At day 0, 200.000 cells were plated in cell culture Petri dishes (Nunc™ 150350, 100x15mm (ThermoFisher) coated with collagen in GM at a density of 3,527

cells/cm2. At day 1, 2 and 3 after plating, the cells were counted, at least in duplicate independent dilutions, using the automated cell counter Countess™ (Invitrogen) and Eve™ cell counting slides (NanoEntek). For each time point one different plate was included and the cells were no replated after counting. For each primary myoblast culture at least two independent experiments were performed. For *ex vivo* BrdU assay, 1,500 satellite cells isolated by FACs sorting were plated in collagen coated 24 well-plates and grown for 3 days in GM before adding bromodeoxyuridine (BrdU, Sigma-Aldrich) for 1 hour. Immunostaining and quantification was performed as described in [59]. In addition, 4,000 satellite cells-derived primary myoblasts were plated in collagen coated 24 well-plates and grown for 1 day in GM before adding 20 µM of 5-ethynyl-2-deoxyuridine (EdU) for 2 hours. Protocol was performed according to the manufacturer instructions (ThermoFisher Scientific). The cell nuclei were stained with DAPI and analysed using Fortessa cytometer at the Cytometer service of the IGTP, Badalona.

HDAC11 knockdown using shRNA constructs

The shRNA sequences used to downregulate HDAC11 levels were published in [60,61] for shRNA24-HDAC11 and in [19,29,61] for and shRNA28-HDAC11. Control shRNA corresponds to turbo-GFP targeting SHC002 from Addgene. The corresponding shRNA sense and antisense sequences were purchased as oligonucleotides from Life technologies (Invitrogen) and cloned into pLKO following Addgene protocol (https://www.addgene.org/tools/protocols/plko/) and verified by Sanger sequencing. To produce lentivirus, 293T cells were transfected using $CaPO_4$ method using 10 µg of the corresponding shRNA vector and 3 µg of CMV-VSV-G and 8 µg of psPAX2 as packaging vectors. 72h after transfection the media was collected, filtered using 0.45 µm polysulfonate

filters (Ref. 514-0074, VWR), diluted 1:2 with fresh media and added to C2C12 proliferating cells with 8 µg/ml of polybrene (Hexadimethrine bromide, Ref. H9268, Sigma Aldrich). Stable expressing shRNA cell lines were produced by selecting resistance cells using puromycin and shRNA downregulation efficiencies were assessed by RT-qPCR.

RNA-seq transcriptomic assay

For transcriptomic analysis of D1 differentiating WT and KO myoblasts RNA was extracted using PureLink™ RNA Mini Kit (Ambion, Life Technologies) including On-Column PureLink® DNase treatment. Library preparation was performed at the High Content Genomics and Bioinformatics Unit of IGTP, Badalona. RNA integrity was assessed by Bioanalyzer nano 6000 assay and all samples had RNA integrity number (RIN) values between 8 and 9.4. Stranded mRNA sequencing libraries were generated with the NEBNext® Ultra™ Directional RNA Library Prep Kit for Illumina starting from 100 ng of total RNA subjected to oligo-dT capture with the NEBNext Poly (A) mRNA Magnetic Isolation Module. Libraries obtained had an average size range between 344 and 424 bp as determined by Bioanalyzer DNA 1000 assay. Libraries were quantified by qPCR with the KAPA library quantification kit for Illumina GA. Sequencing was performed at the Genomics Unit of the Center for Genomic Regulation (CRG) on an Illumina HiSeq2500 sequencer using TruSeq v4 chemistry to generate between 46 and 62 million 2x50 bp paired end reads per sample.

Bioinformatics and statistical analysis were performed at the High Content Genomics and Bioinformatics Unit at the IGTP, Badalona and details are in Supplemental Information. Data was deposited in NCBI's Gene Expression Omnibus accessible through GEO Series accession number GSE147423, https://www.ncbi.nlm.nih.gov/geo/query/acc.cgi?acc=GSE147423).

Analysis of DNA methylation by bisulfite sequencing

Genomic DNA was isolated as described in [62]. Bisulfite conversion was performed using 400 ng of genomic DNA with EZ DNA Methylation™ Kit (ZymoResearch, Orange, CA,) according to manufacturer's protocol. Bisulfite sequencing was performed following Dr. Clark's procedure [63]. PCR amplification was first performed on 1 µl of bisulfite-treated DNA with conventional PCR method in a final volume of 12.5µl, in duplicate, using GTTATAGATGGTATAGGAATGTAGGG as forward and AAATCCCCAAAACCCATACTTAACC as reverse primers. These PCR products were used directly as templates for a nested PCR with conventional PCR method using as internal primers forward TAGGAAAGAATATATAGTTGGGTTGG and reverse CCCAAAACCCATACTTAACCCCAC. The generated amplicons were checked by DNA electrophoresis in 2% agarose stained with ethidium bromide and cleaned by incubating 5µl of each sample with 10 U of Exonuclease I and 1 U of FastAP™ alkaline phosphatase (Ref. EF0654, Thermo Scientific) at 37ºC for 15 min, followed by 85ºC for 15 min of inactivation. The purified products were checked again by DNA electrophoresis and sequenced with the internal reverse primer at GATC Biotech service (Constance, Germany). The results were represented using Methylation plotter (http://maplab.imppc.org/methylation_plotter/ [64] and the primers were designed using MethPrimer [65].

Chromatin immunoprecipitation (ChIP) assay

For ChIP analysis, differentiated cells at 24h were cross-linked by adding 1% formaldehyde directly to cell media for 10 min at RT with shacking (Ref. K41839403, Merck). After 10 minutes, unreacted formaldehyde was quenched by adding fresh glycine at a final

concentration of 0.125 M for 5 min at RT with shacking (Ref. 68790, Sigma-Aldrich). The media was then discarded and the plates were washed twice on ice with PBS 1X containing protease inhibitors (Complete, Mini Protease inhibitor cocktail, Ref. 11836153001, Sigma-Aldrich), scrapped and stored at -80ºC until processing using MagnaChIP A/G kit following the manufacturer´s protocol (Ref. 17-10086, Millipore). Briefly, the resulting lysates were sonicated using Bioruptor (Diagenode) to shear the DNA to fragment lengths of 200 to 500 base pair. For each immunoprecipitation reaction, 50 µg of shared chromatin were diluted 10 folds with dilution buffer and mixed with 20 µl Magna ChIP™ Protein A+G Magnetic Beads (Ref. 16-663, Merck-Millipore) and incubated o/n at 4ºC with the following antibodies: 10 µl α-H3 (cat# ab1791, Abcam), 5 µg α -panH3ac (cat# 06-599, Upstate-Millipore), 5 µg α-H3K9ac (Millipore, cat# 07-352) and 5 µg of normal rabbit IgG (cat# CS200581, Millipore). Next day, beads were washed once with low salt buffer, high salt buffer and LiCl buffer and twice with TE. After de-crossling of the immunoprecipitated samples and inputs, DNA was purified using JETQuick columns following the manufacture's protocol. Samples were quantified by qPCR using LightCycler 480 PCR (Roche) in triplicates. Relative amount of immunoprecipitated marks were calculated as the amount of amplified DNA normalized to the corresponding input values or by total H3 levels. Primers were design using Primer3 (v. 0.4.0) (http://frodo.wi.mit.edu/). The primer sequences are in Supplemental Information Table 2.

Gene expression analysis

Total RNA from skeletal muscle tissue, C2C12 cells and satellite cell-derived mouse and human primary myoblasts were extracted using PureLink™ RNA Mini Kit (Ref. 12183018A,

Ambion, Life Technologies), including ON-Column PureLink®DNase treatment and quantified using Nanodrop (ThermoScientific). Integrity was checked by observation of 28S and 18S ribosomic bands on 1% agarose gel electrophoresis stained with SYBR Green. Total RNA from FACS-sorted macrophages were extracted using PicoPure RNA Isolation Kit (Catalog # KIT0202, Appliedbiosystems) and quantified and checked using Bioanalyzer Instrument. For each sample, 500 ng or 40 ng (for macrophage cells) of total RNA was then reverse transcribed by SuperScript ™ III, following the manufacturer's protocol. RNA expression levels were analysed using the quantitative Real Time PCR technique in the LightCycler®480 (Roche Diagnostics Corporation) platform. Each sample was run in triplicates. Samples without reverse transcriptase during cDNA conversion were also assessed to ensure that there was no DNA contamination. Primers were designed using the Integrated DNA Technologies (IDT) tool (http://eu.idtdna.com/scitools/Applications/RealTimePCR/) and are listed in Supplemental Information Table 3 (mouse) and Table 4 (human). Primer efficiency was calculated by extracting fluorescence raw data and using the Chainy tool (http://maplab.imppc.org/chainy/; [66]) and two different references genes were used for each experiment.

Histology and immunohistochemistry

Tibialis Anterior (TA) and Gastrocnemius (GC) muscles were dissected, embedded in OCT compound (ref. 00411243, VWR), frozen in isopentane precooled with liquid nitrogen and stored at −80 °C. Serial sections of 10µm-thick were cut in a cryostat, collected on SuperFrost®Plus microscope slides (Ref. 631-0108, VWR) and stored at −80°C. TA and GC sections were processed for hematoxylin and eosin staining using conventional methods to

analyse muscle histology. For TA immunohistochemical identification of PAX7, KI67, MYOG and LAMININ, slides were defrosted and equilibrated at room temperature (RT) for 15 min and hydrated by washing with PBS 1X. Cryosections were fixed in 4% paraformaldehyde for 20 min at RT, rinsed three times for 5 min with PBS and fixed again in cold methanol for 6 min at -20 ºC. Sections were rinsed three times with PBS and antigen retrieval was performed for 10 min at 100°C (citric acid 10mM pH= 6 and 0,05% Tween-20). Sections were rinsed three times with PBS and blocked in PBS supplemented with 10% goat serum, 5% BSA (IgG free) at RT for 2 h. A second blocking step was performed on M.O.M. Ig blocking reagent (Catalog No. PK-2200, Vector Laboratories) for 30 min at RT. Incubation with primary antibodies was carried out overnight at 4°C (information of each antibody used is described in Supplemental Information Table 5). The next day, sections were rinsed three times with PBS + 0.025% Tween-20 for 5 minutes followed by incubation with secondary antibodies coupled to Alexa 488 or Alexa-568 for 1 h a RT. Sections were rinsed again with PBS + 0.025% Tween-20 and nuclei were counterstained with DAPI (1 µg/ml) in PBS during 10 min before mounting with Fluoromount (Sigma-Aldrich). Slides were stored at 4°C until analysis.

For immunohistochemical identification of eMYHC in TA and GC muscles, slides were defrosted and equilibrated at RT for 15 min and hydrated by washing with PBS 1X. Internal peroxidases were blocked by incubation with 3% H_2O_2 in PBS for 30 min (Ref. H1009, Sigma-Aldrich) and then washed twice with PBS for 3 min each. Sections were blocked on M.O.M. Ig blocking reagent (Catalog No. PK-2200, Vector Laboratories). Then, they were washed twice with PBS for 3 min and incubated at RT for 1 h with primary antibodies against eMYHC (F1652, Developmental Studies Hybridoma Bank). Slides were washed for 3 min with 0.1 %

Tween PBS and then incubated for 20 min at RT with 1/250 v/v secondary biotinylated α-mouse IgG diluted in 8 % v/v M.O.M. protein concentrate in PBS 1X. Sections were then washed twice for 3 min with 0.1 % Tween PBS 1X, followed by incubation for 15 min at RT with ABC (avidin/biotin) M.O.M solution. Two washes were performed for 3 min with 0.1 % Tween and finally, the staining was developed by incubation with 0.6% 3,3'-diaminobenzidine (DAB) in PBS under the microscope until brown coloration was clearly observed. The slides were immediately mounted with DPX (Ref. 44581, Sigma-Aldrich). The secondary antibody specificity was tested by incubation in the absence of primary antibody.

Differentiation and fusion assays

For differentiation assay 4,000 satellite cell-derived primary myoblasts were cultured on matrigel coated 24-well plates and kept in GM. Next day GM was replaced for DM and 24 hours later MYOG staining was performed: differentiating cells were fixed in 3.7% formaldehyde for 10 min at RT, and rinsed three times with PBS 1X before permeabilization with 0.5% Triton in PBS for 10 min. Next, cells were rinsed three times with PBS 1X and blocked with PBS supplemented with 10% goat serum, 5% BSA (IgG free) at RT for 1 h. Incubation with MYOG antibody (sc12732, Santa Cruz, dilution 1/300) was carried out overnight at 4°C. The next day, cells were rinsed three times with PBS + 0.025% Tween-20 for 5 minutes followed by incubation with anti-mouse secondary antibody coupled to Alexa 488 (Ref. 115-545-205, Jackson Immune Research, 1/400) for 1 h a RT in darkness. Cells were rinsed again with PBS + 0.025% Tween-20 and nuclei were counterstained with DAPI (1 µg/ml) in PBS during 10 min. Cells were kept in PBS + 0,02% sodium azide and positive

staining was visualized and counted using a Leica DMI 6000 B microscope. At least three biological replicates were done per genotype.

For fusion assay 12,000 satellite cell-derived primary myoblasts were cultured on matrigel coated 24-well plates and kept in GM. Next day GM was replaced for DM and 3 days later eMYHC staining was performed: differentiated cells were fixed in 3.7% formaldehyde for 10 min at RT, and rinsed three times with PBS 1X before blocking with TNB buffer (NEN Life Science Products) at RT for 1 h. The cells were then incubated with an antibody against eMYHC (F1.652, neat hybridoma supernatant; Developmental Studies Hybridoma Bank) for 1 h at room temperature. Cells were washed in PBS with 0.1% Tween, and then incubated in biotinylated goat anti–mouse antibody (Jackson Immuno Research Laboratories). Number of nuclei in eMYHC-positive cells was counted and expressed as a percentage of the total number of nuclei analysed. The fusion index was determined by dividing the number of nuclei in eMYHC-positive myotubes divided by the total number of nuclei. At least three biological replicates were done per genotype.

Western blot analysis

Mouse tissues were homogenized using a TissueRuptor (Qiagen) in ice-cold RIPA buffer (150 mM NaCl, 1% Triton X-100, 0.5% deoxycholate, 0.1% SDS and 50 mM Tris pH7.4 supplemented with 2µg/ml Aprotinin, 30mM PMSF, 1mM Sodium orthovanadate, 5mM Sodium fluoride (NAF) and 2µg/ml Pepstatin A). Protein lysates were obtained collecting supernatants after centrifugation at 16,000 g for 30 min at 4ºC. Protein concentrations were determined by BCA method (Ref. 23225, Pierce™ BCA Protein Assay Kit). For each sample, 40-50 µg of protein extract were separated by 8% SDS-polyacrylamide electrophoresis and

electrotransferred to polyvinylidene difluoride (PVDF) membranes (Ref. IPH00010, Millipore). Total levels of protein transferred to membranes were detected using Sypro Ruby protein blot stain as described by the manufacturer (Ref. S11791, ThermoFisher Scientific). Membranes were blocked in 5% non-fat milk in 0.1% Tween TBS 1X (248 mM Tris, 1.37 M NaCl and 26.83 mM KCl, pH8) for 1 hour and probed with the primary antibody against HDAC11 overnight at 4ºC (1/400; sc390737, Santa Cruz). After incubation, four washes with 0.1% Tween TBS 1X for 5 min each were performed. Then, membranes were incubated with the HRP-conjugated secondary antibody (1/10000; P0447, Dako) for 60 min at room temperature. After incubation, four washes with 0.1% Tween TBS 1X for 5 min each were performed. Membranes were scanned in Fuji Film Processor FPM-100A. Total protein staining was used as loading control (Sypro Ruby protein blot stain, Invitrogen).

Statistical analysis

Statistical significance was assess using the statistical package included in GraphPad Prism 6 software. Experimental groups were compared by two-tailed unpaired and paired Student's t test or ANOVA. The data in the graphs represent the mean ± SD of independent experiments. A p value < 0.05 was considered significant (*p < 0.05; **p < 0.001; ***p < 0.0001).

Figure legends

Figure 1. HDAC11 is the HDAC member with maximal gene-expression induction at the onset of satellite-cell differentiation

A) Microarray data showing expression fold change (FC) of all HDAC family members between day 1 differentiating (D1) and proliferating (P) satellite-cell-derived primary myoblasts. **B)** Microarray validation by RT-qPCR of classical HDACs in differentiating (D1) and proliferating (P) satellite-cell-derived primary myoblasts. **C)** Expression level of HDAC11, by RT-PCR, in differentiation time-courses in mouse and human satellite-cell-derived primary myoblasts (left and middle grafts, respectively), and in C2C12 cell line (right graft). Data represent the average of four independent sets of satellite cell-derived primary myoblasts for mouse samples and two for human samples ± SD. ND means not detected. Three independent technical replicates were performed for C2C12 cells. Paired t-test with two tails was applied to assess statistical significance. *: p val <0.05; **: p val < 0.01. **D)** ENCODE ChIP-seq bigwig tracks of MYOD, MYOG and E-proteins TCF3 and TCF12 at proliferation and differentiation points. Data visualized using WashU Epigenome Browser browser v40.6 mm9**.**

Figure 2. HDAC11 is dispensable for adult skeletal muscle growth and homeostasis

A) Left: Representative image of a tibialis (TA) and gastrocnemius (GC) muscles from HDAC11 wild-type (WT) and knock-out (HDAC11$^{-/-}$) mice. Right: Average weight in grams of TA and GC muscles ± SD. **B)** Left: Hematoxylin/eosin (H/E) representative sections of TA and GC muscles from WT and HDAC11$^{-/-}$ mice. Right: Average values of male and female myofiber cross-sectional areas (CSA) and number of myofibers/mm^2. Scale bar: 100 µm. **C)**

Left: Representative sections of TA muscles from WT and HDAC11$^{-/-}$ mice stained with PAX7 (green) and DAPI (blue). Arrows indicate SCs that are PAX7^{+}/DAPI^{+}. Right: Quantification of PAX7^{+} SC number per 100 fibers. Scale bar: 25 µm. Data information: n = 4-6 mice of three months of age for each group. In (B) and (C) a minimum of 400 myofibers were analysed per muscle and animal. Data are represented as means ± SD and statistical significance was determined by unpaired t-test with two tails.

Figure 3. Skeletal muscle regeneration is accelerated in HDAC11-deficient mice

A) Top: Hematoxylin/eosin (H/E) representative sections of tibialis anterior (TA) muscles from WT and HDAC11$^{-/-}$ male mice at the indicated points after injury. Scale bar: 100 µm. Bottom: Average cross-sectional area (CSA) of the central-nucleated regenerating fibers (CNFs) at the same time points after injury, and regenerating fiber size distribution represented as percentage of CNFs in the indicated area intervals. **B)** Left: Representative sections of TA male muscles stained with embryonic myosin heavy chain (eMYHC) to visualize regenerating fibers at 4 and 7 days post injury. Scale bar: 100 µm. Inset: 25 µm. Right: Average cross-sectional area (CSA) of eMYHC-positive myofibers at the same time points after injury, and regenerating fiber size distribution represented as percentage of eMYHC^{+} myofibers in the indicated area intervals. Data information: n = 3-5 mice of 3 months of age for each group. A minimum of 300 CNFs were analysed per muscle and animal using at least 5 random images per animal. Data are represented as means ± SD. Statistical significance was determined by unpaired t-test with two tails for CSA data and by two-way ANOVA test for distribution of CNFs; **: p val <0.01.

Figure 4. HDAC11 deficiency alters satellite-cell differentiation kinetics during skeletal muscle regeneration

A-B) Left: Representative sections of tibialis anterior muscles from WT and HDAC11$^{-/-}$ mice at 7dpi **(A)** and 21dpi **(B)**. Muscles were stained with PAX7 (green), KI67 (red) and DAPI (blue) or MYOG (green), LAMININ (red) and DAPI (blue). Arrows indicate SCs that are PAX7^{+}/KI67^{+}/DAPI^{+}. Scale bar: 25 µm. Right: Quantification of PAX7^{+} SCs number, PAX7^{+}/KI67^{+} SCs number and MYOG^{+} SCs number per 100 CNFs. **C)** Quantification of PAX7^{+} SCs number, PAX7^{+}/KI67^{+} SCs number and MYOG^{+} SCs number per 100 CNFs in not injured (NI), 4, 7, 21 and 60 days post injured WT and HDAC11$^{-/-}$ muscles. Data information: n = 3-6 male mice of three month of age for each group. A minimum of 300 CNFs were analysed per muscle and animal. Data are represented as means ± SD and statistical significance was determined by unpaired t-test with two tails. *: p val <0.05.

Figure 5. Satellite cell-intrinsic loss of HDAC11 enhances myogenic differentiation

A) Left: Growth curves of WT and HDAC11$^{-/-}$ freshly isolated satellite cells after 24, 48 and 72 hours growing in proliferation medium. Values represent the average value of counts at each time point ± SD. Right: Percentage of the freshly isolated primary myoblasts incorporating 5-bromodeoxyuridine (BrdU) labelling after 3 days growing in proliferation medium. **B)** Left: representative images of immunofluorescence staining with MYOG (green) and DAPI (blue) of WT and HDAC11$^{-/-}$ satellite cell-derived primary myoblasts, at 24 hours of differentiation. Scale bar: 50 µm. Right: Percentage of MYOG^{+} cells in WT and HDAC11-deficient satellite cell-derived primary myoblasts, at 24 hours of differentiation. **C)** Left: representative images of day 3 differentiated HDAC11 WT and HDAC11$^{-/-}$ satellite cell-

derived primary myoblasts stained with embryonic myosin (eMYHC). Right: Quantification of fusion index, calculated as the number of myonuclei in eMYHC + myotubes divided by the total number of nuclei. Scale bar: 100 µm. **D)** RT-qPCR quantification of *Myomaker* (*Mymk*), *Myomixer* (*Mymx*) and *Dysferlin* (*Dysf*) expression levels from WT and HDAC11$^{-/-}$ satellite cell-derived primary myoblasts at day 3 of differentiation. WT expression reference value = 1. Data information: n = 3-4 mice of three months of age from which were sorted freshly isolated satellite cells and growth as indicated. Data are represented as means ± SD and statistical significance was determined by t-test with two tails; *: p val <0.05.

Figure 6. HDAC11$^{-/-}$ myoblasts express higher levels of cell cycle-related genes and exhibit sustained proliferation in differentiating conditions

A) Graphical representation of the 7 top statistically significant gene ontology (GO) terms enriched in gens overexpressed (dark green bars) or downregulated (light green bars) in HDAC11$^{-/-}$ day 1 differentiating myoblasts compared to WT counterparts. **B)** Independent RT-qPCR validation of selected genes (identified as upregulated by RNA-seq in mouse HDAC11$^{-/-}$ myocytes) in C2C12 cell lines expressing non-mammalian targeting (shCtr) and HDAC11 targeting shRNAs. Data show HDAC11 depletion and upregulation of the indicated targets measured in three independent experiments ± SD. **C)** Quantification of mRNA levels by RT-qPCR of different sarcomere-related genes and calcium sensing/releasing-related genes in TA muscles from WT and HDAC11$^{-/-}$ three-month old mice. WT expression reference value = 1. **D)** FACS quantification of the proportion of EdU stained cells at 6, 12 and 36 hours after induction cell differentiation in WT and HDAC11$^{-/-}$ satellite cell-derived primary myoblasts. Data represents the average values of three independent experiments ± SD. **E)** Quantification

of expression level by RT-qPCR of HDAC11 in C2C12 cell lines expressing non-mammalian targeting (shCtr) and HDAC11 targeting shRNAs at 1 day of differentiation. On the same cells, the expression level of *Aurka*, *Aurkb* and *Pcna* genes was determined by RT-qPCR before performing ChIP assays. Data represents the average of three independent experiments ± SD. Paired and unpaired t-test with two tails was applied to assess statistical significance between groups. *: p val <0.05. For each gene (*Aurka*, *Aurkb* and *Pcna*) a representative experiment of ChIP qPCR analysis for PanH3ac and H3K9ac, in the corresponding promoter regions, is shown**.** ChIP data were normalized to the corresponding input values.

Figure 7. HDAC11-deficient macrophages overexpress IL-10.

A) Representative FACS plots and gating schemes to isolate macrophages populations of muscle extracts as described in [58]. **B)** Percentage of total isolated macrophage subpopulations M1 and M2 from WT and HDAC11$^{-/-}$ muscles extracts at 4 and 7 days post injury (dpi). **C)** Quantification of expression levels of indicated cytokines by RT-qPCR from M1 isolated macrophages at 4 dpi. **D)** Quantification of expression levels of indicated cytokines by RT-qPCR from M2 isolated macrophages at 4 and 7 dpi. Data information: n = 4 male mice of three old age for each group. Data are represented as means ± SD and statistical significance was determined by unpaired t-test with two tails. *: p val <0.05; **: p val <0.01.

Acknowledgments

We thank Vera Lukesova, Rosa Mª Ampudia, Mar Garcia-Colomer, and Drs. Mercè Jardí and Sara Capdevila for excellent technical assistance. We thank Victoria Moiseeva for kindly helping with FACS sorting experiments, Erica Ramírez and Dr. Òscar Fornas for technical assistance in Flow Cytometry Unit at PRBB and Gerard Requena and Dr. Marco Antonio Fernández for technical assistance in Flow Cytometry Unit at IGTP. This work was supported by *Ministerio de Economía y Competitividad* (BFU2016-80748 to M.S. and BFU2017-89408-R to A.M.P.) and *Ministerio de Ciencia, Innovación y Universidades* (RTI2018-094009-B-I00 to M.A.P.), Feder funds, Generalitat de Catalunya (2017 SGR969 and 2017 SGR206) and Junta de Castilla y Leon (CSI239P18). Y.N.A was supported by FPU12/05668 and E.H. was supported in part by BFU2016-80748 project.

Author contributions

Y. Núñez-Álvarez and E. Hurtado designed and carried out experiments and data analysis. M Muñoz and I. Tuñon gave technical assistance. R. Pluvinet performed RNA-seq experiments. A. M. Pendás generated the HDAC11-deficient mice. G. Reich and L. Sumoy performed the bioinformatics' analysis of RNA-seq data. M.A. Peinado revised the manuscript. M. Suelves conceived the experiments and wrote the manuscript. All the authors contributed with critical discussions and read and approved the final version of the manuscript.

Disclosure of potential conflicts of interest

The authors declare that they have not competing interest.

References

1 Bentzinger CF, Wang YX, Dumont NA & Rudnicki MA (2013) Cellular dynamics in the muscle satellite cell niche. *EMBO Rep.* **14**, 1062–1072.

2 Seale P, Sabourin LA, Girgis-Gabardo A, Mansouri A, Gruss P & Rudnicki MA (2000) Pax7 is required for the specification of myogenic satellite cells. *Cell* **102**, 777–786.

3 Brack AS & Rando TA (2012) Tissue-specific stem cells: Lessons from the skeletal muscle satellite cell. *Cell Stem Cell* **10**, 504–514.

4 Tidball JG (2017) Regulation of muscle growth and regeneration by the immune system. *Nat. Rev. Immunol.* **17**, 165–178.

5 Kharraz Y, Guerra J, Mann CJ, Serrano AL & Muñoz-Cánoves P (2013) Macrophage plasticity and the role of inflammation in skeletal muscle repair. *Mediators Inflamm.* **2013**, 491497.

6 Seto E & Yoshida M (2014) Erasers of histone acetylation: the histone deacetylase enzymes. *Cold Spring Harb. Perspect. Biol.* **6**, a018713.

7 Gao L, Cueto MA, Asselbergs F & Atadja P (2002) Cloning and functional characterization of HDAC11, a novel member of the human histone deacetylase family. *J. Biol. Chem.* **277**, 25748–25755.

8 Gregoretti I, Lee Y-M & Goodson H V (2004) Molecular Evolution of the Histone Deacetylase Family: Functional Implications of Phylogenetic Analysis. *J. Mol. Biol.* **338**, 17–31.

9 Carrió E, Díez-Villanueva A, Lois S, Mallona I, Cases I, Forn M, Peinado MA SM (2015) Deconstruction of DNA Methylation Patterns During Myogenesis Reveals Specific Epigenetic Events in the Establishment of the Skeletal. *Stem Cells* **33**, 2025–2036.

10 Haberland M, Arnold MA, McAnally J, Phan D, Kim Y & Olson EN (2007) Regulation of HDAC9 Gene Expression by MEF2 Establishes a Negative-Feedback Loop in the Transcriptional Circuitry of Muscle Differentiation. *Mol. Cell. Biol.* **27**, 518–525.

11 Dressel U, Bailey PJ, Wang SCM, Downes M, Evans RM & Muscat GEO (2001) A Dynamic Role for HDAC7 in MEF2-mediated Muscle Differentiation. *J. Biol. Chem.* **276**, 17007–17013.

12 The ENCODE Project (2012) An integrated encyclopedia of DNA elements in the human genome. *Nature* **489**, 57–74.

13 Cao Y, Yao Z, Sarkar D, Lawrence M, Sanchez GJ, Parker MH, MacQuarrie KL, Davison J, Morgan MT, Ruzzo WL, Gentleman RC & Tapscott SJ (2010) Genome-wide MyoD Binding in Skeletal Muscle Cells: A Potential for Broad Cellular Reprogramming. *Dev. Cell* **18**, 662–674.

14 Suelves M, Vidal B, Serrano AL, Tjwa M, Roma J, López-Alemany R, Luttun A, De Lagrán MM, Díaz MÀ, Jardí M, Roig M, Dierssen M, Dewerchin M, Carmeliet P & Muñoz-Cánoves P (2007) uPA deficiency exacerbates muscular dystrophy in MDX mice. *J. Cell Biol.* **178**, 1039–1051.

15 Vidal B, Serrano AL, Tjwa M, Suelves M, Ardite E, De Mori R, Baeza-Raja B, De Lagrán MM, Lafuste P, Ruiz-Bonilla V, Jardí M, Gherardi R, Christov C, Dierssen M, Carmeliet P, Degen JL, Dewerchin M & Muñoz-Cánoves P (2008) Fibrinogen drives dystrophic muscle fibrosis via a TGFβ/alternative macrophage activation pathway. *Genes Dev.* **22**, 1747–1752.

16 Chazaud B, Brigitte M, Yacoub-Youssef H, Arnold L, Gherardi R, Sonnet C, Lafuste P & Chretien F (2009) Dual and beneficial roles of macrophages during skeletal muscle

regeneration. *Exerc. Sport Sci. Rev.* **37**, 18–22.

17 Arnold L, Henry A, Poron F, Baba-Amer Y, Van Rooijen N, Plonquet A, Gherardi RK & Chazaud B (2007) Inflammatory monocytes recruited after skeletal muscle injury switch into antiinflammatory macrophages to support myogenesis. *J. Exp. Med.* **204**, 1057–1069.

18 Perdiguero E, Sousa-Victor P, Ruiz-Bonilla V, Jardí M, Caelles C, Serrano AL & Muñoz-Cánoves P (2011) p38/MKP-1-regulated AKT coordinates macrophage transitions and resolution of inflammation during tissue repair. *J. Cell Biol.* **195**, 307–322.

19 Villagra A, Cheng F, Wang HW, Suarez I, Glozak M, Maurin M, Nguyen D, Wright KL, Atadja PW, Bhalla K, Pinilla-Ibarz J, Seto E & Sotomayor EM (2009) The histone deacetylase HDAC11 regulates the expression of interleukin 10 and immune tolerance. *Nat. Immunol.* **10**, 92–100.

20 Woods DM, Woan K V., Cheng F, Sodré AL, Wang D, Wu Y, Wang Z, Chen J, Powers J, Pinilla-Ibarz J, Yu Y, Zhang Y, Wu X, Zheng X, Weber J, Hancock WW, Seto E, Villagra A, Yu XZ & Sotomayor EM (2017) T cells lacking HDAC11 have increased effector functions and mediate enhanced alloreactivity in a murine model. *Blood* **130**, 146–155.

21 Sahakian E, Powers JJ, Chen J, Deng SL, Cheng F, Distler A, Woods DM, Rock-Klotz J, Sodre AL, Youn JI, Woan K V., Villagra A, Gabrilovich D, Sotomayor EM & Pinilla-Ibarz J (2015) Histone deacetylase 11: A novel epigenetic regulator of myeloid derived suppressor cell expansion and function. *Mol. Immunol.* **63**, 579–585.

22 Deng B, Wehling-Henricks M, Villalta SA, Wang Y & Tidball JG (2012) IL-10 Triggers Changes in Macrophage Phenotype That Promote Muscle Growth and Regeneration. *J. Immunol.* **189**, 3669–3680.

23 Lu J, McKinsey TA, Zhang C-L & Olson EN (2000) Regulation of Skeletal Myogenesis by

Association of the MEF2 Transcription Factor with Class II Histone Deacetylases. *Mol. Cell* **6**, 233–244.

24 Potthoff MJ, Wu H, Arnold MA, Shelton JM, Backs J, McAnally J, Richardson JA, Bassel-Duby R & Olson EN (2007) Histone deacetylase degradation andMEF2 activation promote the formation of slow-twitch myofibers. *J. Clin. Invest.* **117**, 2459.

25 Li Zhang C, McKinsey TA & Olson EN (2001) The transcriptional corepressor MITR is a signal-responsive inhibitor of myogenesis. *Proc. Natl. Acad. Sci. U. S. A.* **98**, 7354–7359.

26 Wamstad JA, Alexander JM, Truty RM, Shrikumar A, Li F, Eilertson KE, Ding H, Wylie JN, Pico AR, Capra JA, Erwin G, Kattman SJ, Keller GM, Srivastava D, Levine SS, Pollard KS, Holloway AK, Boyer LA & Bruneau BG (2012) Dynamic and coordinated epigenetic regulation of developmental transitions in the cardiac lineage. *Cell* **151**, 206–220.

27 Gan L, Schwengberg S & Denecke B (2014) Transcriptome analysis in cardiomyocyte-specific differentiation of murine embryonic stem cells reveals transcriptional regulation network. *Gene Expr. Patterns* **16**, 8–22.

28 Liu H, Hu Q, Kaufman A, D'Ercole AJ & Ye P (2008) Developmental expression of histone deacetylase 11 in the murine brain. *J. Neurosci. Res.* **86**, 537–543.

29 Watanabe Y, Khodosevich K & Monyer H (2014) Dendrite Development Regulated by the Schizophrenia-Associated Gene FEZ1 Involves the Ubiquitin Proteasome System. *Cell Rep.* **7**, 552–564.

30 Bagui TK, Sharma SS, Ma L & Jack Pledger W (2013) Proliferative status regulates HDAC11 mRNA abundance in nontransformed fibroblasts. *Cell Cycle* **12**, 3433–3441.

31 Glozak MA & Seto E (2009) Acetylation/deacetylation modulates the stability of DNA

replication licensing factor Cdt1. *J. Biol. Chem.* **284**, 11446–11453.

32 Joshi P, Greco TM, Guise AJ, Luo Y, Yu F, Nesvizhskii AI & Cristea IM (2013) The functional interactome landscape of the human histone deacetylase family. *Mol. Syst. Biol.* **9**, 1–21.

33 Moresi V (2015) New insights into the epigenetic control of satellite cells. *World J. Stem Cells* **7**, 945.

34 Kutil Z, Novakova Z, Meleshin M, Mikesova J, Schutkowski M & Barinka C (2018) Histone Deacetylase 11 Is a Fatty-Acid Deacylase. *ACS Chem. Biol.* **13**, 685–693.

35 Moreno-Yruela C, Galleano I, Madsen AS & Olsen CA (2018) Histone Deacetylase 11 Is an ε-N-Myristoyllysine Hydrolase. *Cell Chem. Biol.* **25**, 849-856.e8.

36 Blais A, Tsikitis M, Acosta-alvear D, Blais A, Tsikitis M, Acosta-alvear D, Sharan R, Kluger Y & Dynlacht BD (2005) An initial blueprint for myogenic differentiation An initial blueprint for myogenic differentiation. *Genes Dev.* **19**, 553–569.

37 Forcales S V., Albini S, Giordani L, Malecova B, Cignolo L, Chernov A, Coutinho P, Saccone V, Consalvi S, Williams R, Wang K, Wu Z, Baranovskaya S, Miller A, Dilworth FJ & Puri PL (2012) Signal-dependent incorporation of MyoD-BAF60c into Brg1-based SWI/SNF chromatin-remodelling complex. *EMBO J.* **31**, 301–316.

38 Di Padova M, Caretti G, Zhao P, Hoffman EP & Sartorelli V (2007) MyoD acetylation influences temporal patterns of skeletal muscle gene expression. *J. Biol. Chem.* **282**, 37650–37659.

39 Meadows E, Cho JH, Flynn JM & Klein WH (2008) Myogenin regulates a distinct genetic program in adult muscle stem cells. *Dev. Biol.* **322**, 406–414.

40 Haberland M, Montgomery RL & Olson EN (2009) The many roles of histone deacetylases

in development and physiology: implications for disease and therapy. *Nat. Rev. Genet.* **10**, 32–42.

41 Zhang Y, Kwon S, Yamaguchi T, Cubizolles F, Rousseaux S, Kneissel M, Cao C, Li N, Cheng H-L, Chua K, Lombard D, Mizeracki A, Matthias G, Alt FW, Khochbin S & Matthias P (2008) Mice Lacking Histone Deacetylase 6 Have Hyperacetylated Tubulin but Are Viable and Develop Normally. *Mol. Cell. Biol.* **28**, 1688–1701.

42 Byun SK, An TH, Son MJ, Lee DS, Kang HS, Lee E, Han BS, Kim WK, Bae K, Oh K & Lee SC (2017) Molecules and Cells HDAC11 Inhibits Myoblast Differentiation through Repression of MyoD-Dependent Transcription. **40**, 1–10.

43 Wang H, Cheng F, Woan K, Sahakian E, Merino O, Rock-Klotz J, Vicente-Suarez I, Pinilla-Ibarz J, Wright KL, Seto E, Bhalla K, Villagra A & Sotomayor EM (2011) Histone Deacetylase Inhibitor LAQ824 Augments Inflammatory Responses in Macrophages through Transcriptional Regulation of IL-10. *J. Immunol.* **186**, 3986–3996.

44 Lin L, Hou J, Ma F, Wang P, Liu X, Li N, Wang J, Wang Q & Cao X (2013) Type I IFN Inhibits Innate IL-10 Production in Macrophages through Histone Deacetylase 11 by Downregulating MicroRNA-145. *J. Immunol.* **191**, 3896–3904.

45 Stammler D, Eigenbrod T, Menz S, Frick JS, Sweet MJ, Shakespear MR, Jantsch J, Siegert I, Wolfle S, Langer JD, Oehme I, Schaefer L, Fischer A, Knievel J, Heeg K, Dalpke AH & Bode KA (2015) Inhibition of Histone Deacetylases Permits Lipopolysaccharide-Mediated Secretion of Bioactive IL-1 via a Caspase-1-Independent Mechanism. *J. Immunol.* **195**, 5421–5431.

46 Dort J, Fabre P, Molina T & Dumont NA (2019) Macrophages Are Key Regulators of Stem Cells during Skeletal Muscle Regeneration and Diseases. *Stem Cells Int.* **8**, 1–20.

47 Jiang H, Khan S, Wang Y, Charron G, He B, Sebastian C, Du J, Kim R, Ge E, Mostoslavsky R, Hang HC, Hao Q & Lin H (2013) SIRT6 regulates TNF-α secretion through hydrolysis of long-chain fatty acyl lysine. *Nature* **496**, 110–113.

48 Villalta SA, Rinaldi C, Deng B, Liu G, Fedor B & Tidball JG (2011) Interleukin-10 reduces the pathology of mdx muscular dystrophy by deactivating M1 macrophages and modulating macrophage phenotype. *Hum. Mol. Genet.* **20**, 790–805.

49 Nitahara-Kasahara Y, Hayashita-Kinoh H, Chiyo T, Nishiyama A, Okada H, Takeda S & Okada T (2014) Dystrophic mdx mice develop severe cardiac and respiratory dysfunction following genetic ablation of the anti-inflammatory cytokine IL-10. *Hum. Mol. Genet.* **23**, 3990–4000.

50 Madaro L, Torcinaro A, de Bardi M, Contino FF, Pelizzola M, Diaferia GR, Imeneo G, Bouchè M, Puri PL & de Santa F (2019) Macrophages fine tune satellite cell fate in dystrophic skeletal muscle of mdx mice. *PLoS Genet.* **15**, 1–29.

51 Fan X Di, Wan LL, Duan M & Lu S (2018) HDAC11 deletion reduces fructose-induced cardiac dyslipidemia, apoptosis and inflammation by attenuating oxidative stress injury. *Biochem. Biophys. Res. Commun.* **503**, 444–451.

52 Sun L, Marin de Evsikova C, Bian K, Achille A, Telles E, Pei H & Seto E (2018) Programming and Regulation of Metabolic Homeostasis by HDAC11. *EBioMedicine* **33**, 157–168.

53 Sun L, Telles E, Karl M, Cheng F, Luetteke N, Sotomayor EM, Miller RH & Seto E (2018) Loss of HDAC11 ameliorates clinical symptoms in a multiple sclerosis mouse model. *Life Sci. Alliance* **1**, e201800039.

54 Minetti GC, Colussi C, Adami R, Serra C, Mozzetta C, Parente V, Fortuni S, Straino S,

Sampaolesi M, Di Padova M, Illi B, Gallinari P, Steinkühler C, Capogrossi MC, Sartorelli V, Bottinelli R, Gaetano C & Puri PL (2006) Functional and morphological recovery of dystrophic muscles in mice treated with deacetylase inhibitors. *Nat. Med.* **12**, 1147–1150.

55 Consalvi S, Mozzetta C, Bettica P, Germani M, Fiorentini F, Del Bene F, Rocchetti M, Leoni F, Monzani V, Mascagni P, Puri PL & Saccone V (2013) Preclinical studies in the mdx mouse model of duchenne muscular dystrophy with the histone deacetylase inhibitor givinostat. *Mol. Med.* **19**, 79–87.

56 Bettica P, Petrini S, D'Oria V, D'Amico A, Catteruccia M, Pane M, Sivo S, Magri F, Brajkovic S, Messina S, Vita GL, Gatti B, Moggio M, Puri PL, Rocchetti M, De Nicolao G, Vita G, Comi GP, Bertini E & Mercuri E (2016) Histological effects of givinostat in boys with Duchenne muscular dystrophy. *Neuromuscul. Disord.* **26**, 643–649.

57 García-Prat L, Martínez-Vicente M, Perdiguero E, Ortet L, Rodríguez-Ubreva J, Rebollo E, Ruiz-Bonilla V, Gutarra S, Ballestar E, Serrano AL, Sandri M & Muñoz-Cánoves P (2016) Autophagy maintains stemness by preventing senescence. *Nature* **529**, 37–42.

58 Moiseeva V M-CPPE (2019) Simultaneous Isolation of Stem and Niche Cells of Skeletal Muscle: Applicability for Aging Studies. *Methods Mol. Biol.*, 13–23.

59 Perdiguero E, Ruiz-Bonilla V, Gresh L, Hui L, Ballestar E, Sousa-Victor P, Baeza-Raja B, Jardí M, Bosch-Comas A, Esteller M, Caelles C, Serrano AL, Wagner EF & Mũoz-Cánoves P (2007) Genetic analysis of p38 MAP kinases in myogenesis: Fundamental role of p38α in abrogating myoblast proliferation. *EMBO J.* **26**, 1245–1256.

60 Cheng F, Lienlaf M, Perez-Villarroel P, Wang HW, Lee C, Woan K, Woods D, Knox T, Bergman J, Pinilla-Ibarz J, Kozikowski A, Seto E, Sotomayor EM & Villagra A (2014) Divergent roles of histone deacetylase 6 (HDAC6) and histone deacetylase 11 (HDAC11)

on the transcriptional regulation of IL10 in antigen presenting cells. *Mol. Immunol.* **60**, 44–53.

61 Kagey MH, Newman JJ, Bilodeau S, Zhan Y, David A, Berkum NL Van, Ebmeier CC, Goossens J, Peter B, Levine SS, Taatjes DJ, Dekker J, Young R a, Dylantaatjescoloradoedu DJT & Jobdekkerumassmededu JD (2010) Mediator and Cohesin Connect Gene Expression and Chromatin Architecture. *Young* **467**, 430–435.

62 Carrió E, Magli A, Muñoz M, Peinado MA, Perlingeiro R & Suelves M (2016) Muscle cell identity requires Pax7-mediated lineage-specific DNA demethylation. *BMC Biol.* **14**, 1–15.

63 Clark SJ, Statham A, Stirzaker C, Molloy PL & Frommer M (2006) DNA methylation: Bisulphite modification and analysis. *Nat. Protoc.* **1**, 2353–2364.

64 Mallona I, Díez-Villanueva A & Peinado MA (2014) Methylation plotter: a web tool for dynamic visualization of DNA methylation data. *Source Code Biol. Med.* **9**, 11.

65 Li L-C & Dahiya R (2002) MethPrimer: designing primers for methylation PCRs. *Bioinformatics* **18**, 1427–1431.

66 Mallona I, Díez-Villanueva A, Martín B & Peinado MA (2017) Chainy, an universal tool for standardized relative quantification in real-time PCR. *Bioinformatics* **33**, btw839.

Supplemental information

Cell lines

Bioinformatics and statistical analysis performed on RNA-seq data

Table 1: List of antibodies used for satellite cells and M1/M2 macrophages isolation

Table 2: List of primers sequences used for qPCR ChIP analysis.

Table 3: List of primers sequences used for mouse qPCR analysis of mRNA expression.

Table 4: List of primers sequences used for human qPCR analysis of mRNA expression.

Table 5: List of antibodies used for immunohistochemistry detection.

Table 6. Selected genes upregulated in HDAC11-deficient myoblasts at day 1 of differentiation from mitotic cell cycle Gene Ontology category.

Table 7. Selected genes downregulated in HDAC11-deficient myoblasts at day 1 of differentiation from muscle contraction Gene Ontology category.

Supplemental Figure 1. HDAC11 expression in human primary skeletal muscle cells.

Supplemental Figure 2. Epigenetic landscape of *Hdac11* genomic locus.

Supplemental Figure 3. Validation of HDAC11 knockout mice.

Supplemental Figure 4. HDAC11-deficient female mice show accelerated muscle regeneration at 7 days post-injury

Supplemental Figure 5. HDAC11$^{-/-}$ mice do not show differences in satellite cells proliferation or differentiation at 4dpi.

Supplemental Figure 6. HDAC11-deficiency does not alter myoblasts proliferation capacity of muscle primary cell cultures.

Supplemental Figure 7. HDAC11$^{-/-}$ differentiating myoblasts do not show different histone acetylation levels in promoter regions of cell-cycle related genes.

Supporting information

Cell lines

Growth medium (GM) for C2C12 cell culture contained DMEM (Dubelcco's Modified Eagle's Medium, Ref. 11960085) supplemented with 15% of inactivated foetal bovine serum (FBS) (Ref. 10270106), 4 mM of L-glutamine (Ref. 25030024), 2 mM of pyruvate (Ref. 11360039) and 100 U/ml penicillin and 100 µg/ml streptomycin (Ref. 15140122). To induce myogenic differentiation, GM was replaced by differentiation medium (DM) composed by DMEM 1X supplemented with 2% of horse serum, 4mM of L-glutamine, 2mM of pyruvate, 100 U/ml of penicillin and 100 µg/ml streptomycin (all reagents were purchased from Gibco, LifeTechnologies). Satellite cell-derived mouse primary myoblasts were grown on tissue culture dishes coated with 0.05 mg/ml Collagen I from rat tail (Becton and Dickinson) with Ham's F-10 supplemental with 20% inactivated FBS, 5 ng/ml bFGF factor (Ref. 100-18B, Peprotech), 100 U/ml penicillin and 100 µg/ml streptomycin). To induce myotube formation, confluent proliferating satellite cell-derived mouse primary myoblasts were grown on matrigel coated culture dishes (Basement Membrane Matrix, Becton and Dickinson) and switched to DM next day for the indicated days. Human satellite cell-derived primary myoblasts were grown on tissue culture dishes coated with 0.05 mg/ml Collagen I from rat tail (Becton and Dickinson) with GM contained 65% of DMEM 1X and 22% of M-199 (Medium 199 with Earle's BSS) supplemented with 10% inactivated FBS, 1 µg/ml insulin (Ref. I-5500, Sigma-Aldrich), 2 mM glutamine, 100 U/ml penicillin, 100 µg/ml streptomycin, 10 ng/ml EGF (Ref. 100-15, Peprotech), and 25 ng/ml bFGF. To induce cell differentiation, confluent proliferating satellite cell-derived human primary myoblasts were plated on matrigel coated tissue culture dishes and the medium was replaced by DM for the indicated time. All media were changed every 2 days.

Bioinformatics and statistical analysis performed on RNA-seq data

Raw sequencing data was assessed for quality with FastQC (http://www.bioinformatics.babraham.ac.uk/projects/fastqc; [64] and quality based trimming was performed using Trimmomatic (http://www.usadellab.org/cms/?page=trimmomatic;[65]). Trimmed reads were aligned to the mouse reference genome (Ensembl release 85, Mus_musculus.GRCm38.dna.primary_assembly) with Tophat v2.0.8 (http://ccb.jhu.edu/software/tophat/index.shtml, [66]), which uses Bowtie v2 (http://bowtie-bio.sourceforge.net/bowtie2/index.shtml). We provided Tophat with the corresponding Ensembl GFT annotation file (Mus_musculus.GRCm38.85.gtf) containing feature coordinates. The resulting BAM files were further analyzed using the QualiMap software (http://qualimap.bioinfo.cipf.es/; [67]). Aligned reads were counted using FeatureCounts [68] based on annotation at the gene, transcripts and exon level. Differential gene expression analysis between WT and KO mice was performed with the DESeq2 R package [69] with p value correction adjusting for multiple testing by the false discovery rate (FDR) method of Benjamini and Hochberg.

Functional enrichment was assessed with several different tools. First, gene ontology enrichment analysis was performed using the GOrilla web server (http://cbl-gorilla.cs.technion.ac.il/; [70]) on the top significant upregulated and downregulated genes after applying a cutoff of an absolute fold change larger than 1.2 and adjusted p-value under 0.05. We also used Enrichr (http://amp.pharm.mssm.edu/Enrichr/, [71,72]) to search for further functional enrichment.

Table 1. List of antibodies used for satellite cells and M1/M2 macrophages isolation.

Antibody	Manufacturer	Specie	Amount of AB used $10^{\wedge 6}$ cells	Comments
Alexa Fluor® 647 anti-CD34, clone RAM34	BD Biosciences	Rat	3 µl	Positive SC selection
PE/anti-α7-integrin	AbLab	Rat	0,5 µl	Positive SC selection
PE/Cy7 anti-CD45	Biolegend	Rat	0,5 µl	Negative SC selection
PE/Cy7 anti-Sca-1	Biolegend	Rat	0,5 µl	Negative SC selection
FICT anti-CD11b, clone M1/70	BD Pharmigen	Rat	1 µl	Positive macrophages selection
APC/Cyanine7 anti-F4/80, clone BM8	Biolegend	Mouse	0,5 µl	Positive macrophages selection
PE anti-Ly6C, clone AL-21	BD Pharmigen	Mouse	0,5 µl	Positive macrophages selection

Table 2. List of primer sequences used for qPCR ChIP analysis.

Name	F (5'->3')	R (5'->3')	Amplicon length	Genomic location	Relative position to TSS	Comments
ChIP controls						
Actb1 promoter	TCGCTCTCTCGTGGCTAGTA	GGAATGTGGCTGCAAAGAGT	152	chr5:143668149-143668300	(+255:+104)	Positive control H3K9ac
Gene desert Chr6	CTGGACGTGTGGATGTTGTC	CCTCCTGCTTACACCTCAGC	51	chr6:120258781-120258831	ND	Negative control H3K9ac
Targets RNA-seq						
Aurka	CCCATTCCCACAAGAACCTA	AAACGGATAGGGAAGGCTGT	125	chr2:172195801-172195925	(+206:+82)	
Aurkb	GAGCGCCTAGTGGCGTAG	GATAGCGGGCACGTGGAT	104	chr11:68859194-68859297	(+50:+153)	
Pcna	CACCTGGTGAGGTTCACG	TCGTCTCACGTCTCCTTGGT	101	chr2:132078549-132078649	(+368:+268)	

Table 3. List of primer sequences used for mouse qPCR analysis of mRNA expression.

Gene name	F (5'->3')	R (5'->3')	Amplicon lenght (bp)
Actn	GAGAAGGGCTATGAGGATTGG	TCGTAGTCGTGCTGGTTTAAC	146
Arg1	CAATGAAGAGCTGGCTGGTGT	GTGTGAGCATCCACCCAAATG	157
Aurka	GCCCCTTGGAACAGTCTATAG	CTCTGGCTTAATGTCTCTGTGG	142
Aurkb	AGGGAGAACTGAAGATTGCAG	CCCGATGCACCATAGATCTAC	149
Ccl2	GGTCTTCAGCACCTTTGAATG	ATTAAGGCATCACAGTCCGAG	145
Ccl22	TCCCTATGGTGCCAATGTG	CAGATATCTCGGTTCTTGACGG	153
Cd163	AGTCATCTGCACTGGGAAAG	GTAAAACACTTCAAGGCGACC	175
Cd68	CAAAGCTTCTGCTGTGGAAAT	GACTGGTCACGGTTGCAAG	140
Ckmt2	GAAGGGAGGTGGAGAATGTG	GGCTTATCAAACAGAAAGTGGTC	139
Hdac1	TGAGGAGGACCCTGACAAAC	ACCACCTTCTCCCTCCTCAT	100
Hdac2	CATGGTGATGGTGTTGAGGA	TCATGGGAAAATTGACAGCA	151
Hdac3	CGACGCTGAAGAGAGAGGTC	TTTCCTTGTCGTTGTCATGG	92
Hdac4	TTCTGAAGCCTGCGTGTC	GGCATTGGGTCTCTGATGTAG	82
Hdac5	GGTTTGATGCTGTTGAAGGAC	AGATGGCGGTCAAGTCATG	150
Hdac6	CCTAGATGTGTCCCAACCTTG	TGTTCAGAGGCTTCATGGTG	132
Hdac7	CATCTGTGATGCCTCGGAG	CAGCCCCAGTATTTCCTGTG	150
Hdac8	ACCGAATCCAGCAAATCCTC	CAGTCACAAATTCCACAAACCG	149
Hdac9	CGTTCATGTAGCAATGGAAGG	GAGACTGAGGGTGTAATGGAAC	131

Hdac10	TTGTGTACCACGAGGACATG	CTCACAAGCTGACAAACACAG	149
Hdac11	TTACAACCGCCACATCTACC	GACATTCCTCTCCACCTTCTC	118
Il-1b	ACGGACCCCAAAAGATGAAG	TTCTCCACAGCCACAATGAG	139
Il-1ra	AAATCTGCTGGGGACCCTAC	TGAGCTGGTTGTTTCTCAGG	165
Il-6	GAACAACGATGATGCACTTGC	CTTCATGTACTCCAGGTAGCTATG(	154
Il-10	CAAGGAGCATTTGAATTCCC	GGCCTTGTAGACACCTTGGTC	157
Ki67	TTGCAAAATTGAAGTCAAAGAGC	TCAATGATGGTTATTATGTCTCC	132
Mck	AGGCATGGCCCGAGAC	AGATCACGCGAAGGTGGTC	101
Myog	GGTGTGTAAGAGGAAGTCTGTG	TAGGCGCTCAATGTACTGGAT	182
Mymk	CATGTTCTTTGTGGCGTTCTC	CAAGCATTGTGAAGGTCGATC	179
Mymx	CTGTCTGCTCTTTGTCCTCAG	GTACTTTGATGGGCGTTGC	142
Myom1	ACCGAGGAAAAGATAAGAGCAG	CAGACAAAGGAGTATAGCCGG	148
Myom2	ATCTTAGCCATGAGTCGTGTG	AGCTGACCTTCATTTCCTCTG	121
Pcna	GGGTGAAGTTTTCTGCAAGTG	GTACCTCAGAGCAAACGTTAGG	137
Ryr1	TCCGCACCATCCTTTCATC	CGTCCTCATCTTCGCTCTTG	144
Tgfβ1	ATTCCTGGCGTTACCTTGG	CGTGGAGTTTGTTATCTTTGCTG	171
Tmod	GCCCTGAAAGAGAACTCCTATG	CCAGAGATGAAGTTGGACTCC	143
Tnfα	TGGAGTCATTGCTCTGTGAAG	CCTGAGCCATAATCCCCTTTC	149
Trdn	AAGACTCCAAAGATGTCCCAC	AACCCATAGCCATTGTACCC	133
Ttn	CAGCGGAAAGTACACAATTAAGG	CACTGCTCGTTTTCAATACCAC	122
*Tbp1**	GGGAGAATCATGGACCAGAA	CCGTAAGGCATCATTGGACT	113
*Actb**	GATTACTGCTCTGGCTCCTAG	GACTCATCGTACTCCTGCTTG	147

** Reference genes*

Table 4. List of primer sequences used for human qPCR analysis of mRNA expression.

Gene name	F (5'->3')	R (5'->3')	Amplicon lenght (bp)
Hdac11	GTTTCTGTTTGAGCGTGTGG	GGTAGATGTGGCGGTTGTAG	140
*Tbp**	GTGGGGAGCTGTGATGTGAA	TGCTCTGACTTTAGCACCTGT	182
*Rpo**	TTCATTGTGGGAGCAGAC	CAGCAGTTTCTCCAGAGC	156

** Reference genes*

Table 5. List of antibodies used for immunohistochemistry detection.

Antigen	Conjugate	Host	Dilution	Source	Reference
PAX7		Mouse	1/20	Santa Cruz	sc81648
KI67		Rabbit	1/100	Abcam	ab15580
MYOG		Mouse	1/40	Santa Cruz	sc12732
LAMININ		Rabbit	1/500	Sigma-Aldrich	L9393
eMYHC		Mouse	ND	Hybridoma Bank	F1.652
Alexa Fluor	488 dye	Mouse	1/400	Jackson Immuno Research	115-545-205
Alexa Fluor	568 dye	Rabbit	1/400	ThermoFisher	A-21124

ND: non-diluted

Table 6. Selected genes upregulated in HDAC11-deficient myoblasts at day 1 of differentiation from mitotic cell cycle Gene Ontology category.

Family	Function	Gene	FC(KO/WT)	p adj val
	Unknown	KI67	2.31	0.0009
	DNA replication	PCNA	2.08	0.01
	Mitosis	BIRC5	2.33	0.0013
Cyclins	Cell cycle progression	CCNA2	2.44	0.001
		CCNB1	2.74	0.0001
		CCNB2	2.42	0.001
		CCNF	2.52	0.0002
Cyclin dependent kinases	Cell cycle progression	CDK1	2.47	0.0048
		CDKN3	2.28	0.0101
Aurora serine/threonine protein kinases	Chromatid segregation	AURKA	2.58	0.0007
		AURKB	3.05	0.00002
	Initiation of replication	CDT1	2.76	0.0016
		GMNN	2.31	0.0131
Minichromosome maintenance complex	Replicative helicase complex	MCM3	2.59	0.0019
		MCM4	2.19	0.0151
		MCM5	2.89	0.0007
		MCM6	2.2	0.0098
		MCM7	2.15	0.0233
	HRR	MCM8	2.1	0.0026
Constitutive centromere associated network (CCAN)	Kinetochore formation	CENPA	2.58	0.0006
		CENPH	2.68	0.0004
		CENPI	2.71	0.0002
		CENPK	2.15	0.0186
		CENPL	1.99	0.0149
		CENPN	2.08	0.0209
		CENPQ	2.25	0.0003
		CENPU	2.25	0.0101
		CENPW	1.97	0.0091
Other proteins associated to kinetochore	Kinetochore formation	CENPE	2.53	0.0001
		CENPF	2.17	0.0005
		INCENP	2.29	0.0023
Kinesins	Mitosis	KIF2C	2.57	0.0003
		KIF4	2.71	0.00002
		KIF7	1.68	0.0126
		KIF11	2.25	0.0024
		KIF14	2.32	0.0001
		KIF15	2.59	0.0009
		KIF18A	2.59	0.0015
		KIF18B	2.91	0.00004
		KIF20A	2.47	0.0001
		KIF20B	2.29	0.0013

		KIF22	2.48	0.0007
		KIF23	2.62	0.0002
		KIFC1	2.57	0.0003
		KIFC5B	2.07	0.0028
Shugosin-like proteins	Chromatids cohesion	SGOL1	2.54	0.0009
		SGOL2A	2.36	0.00003
Condensin	Chromosome assembly/segregation	SMC2	2.06	0.0063
		SMC4	2.19	0.0002

Table 7. Selected genes downregulated in HDAC11-deficient myoblasts at day 1 of differentiation from muscle contraction Gene Ontology category.

Family	Function	Gene	Alternative name	FC(KO/WT)	p adj val
Contractile proteins	Muscle contraction	MYL1	Myosin light chain 1	-2.76	0.0182
		MYL4	Myosin light chain 4 (atrial, cardiac)	-2.59	0.0167
		MYL6B	Myosin light chain B	-2.51	0.0075
		MYLPF	Myosin light chain, phosphorylable	-2.43	0.0234
Structural proteins	Maintenance of sarcomere structure	ACTN3	α-actinin type 3	-2.51	0.0147
		MYOM1	Skelemin	-2.52	0.0347
		MYOM2	Myomesin2	-2.49	0.0352
		MYOM3	Myomesin3	-2.23	0.0286
		MYPN	Myopalladin	-2.18	0.031
		NEB	Nebulin	-2.58	0.0082
		OBSCN	Obscurin	-3	0.01
		TTN	Titin	-2.12	0.042
Regulatory proteins	Calcium sensing regulation of actin-myosin interaction	PVALB	Parvalbumin	-4.41	0.0004
		TNNI1	Troponin I type 1	-2.8	0.0072
		TNNT3	Troponin T type 3	-2.14	0.0442
		TMOD1	Tropomodulin1	-2.57	0.019
Sarcoplasmatic reticulum	Calcium release	RYR1	Ryanodine receptor1	-2.55	0.003
		TRDN	Triadin	-3.2	0.0037

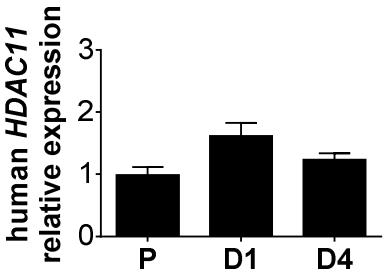

Supplemental Figure 1. HDAC11 expression in human primary skeletal muscle cells.
Expression level of HDAC11, by RT-PCR, in proliferation (P) and at day1 (D1) and day 4 (D4) of differentiation in human satellite-cell-derived primary myoblasts. Data represent the average of two independent sets of human samples ± SD.

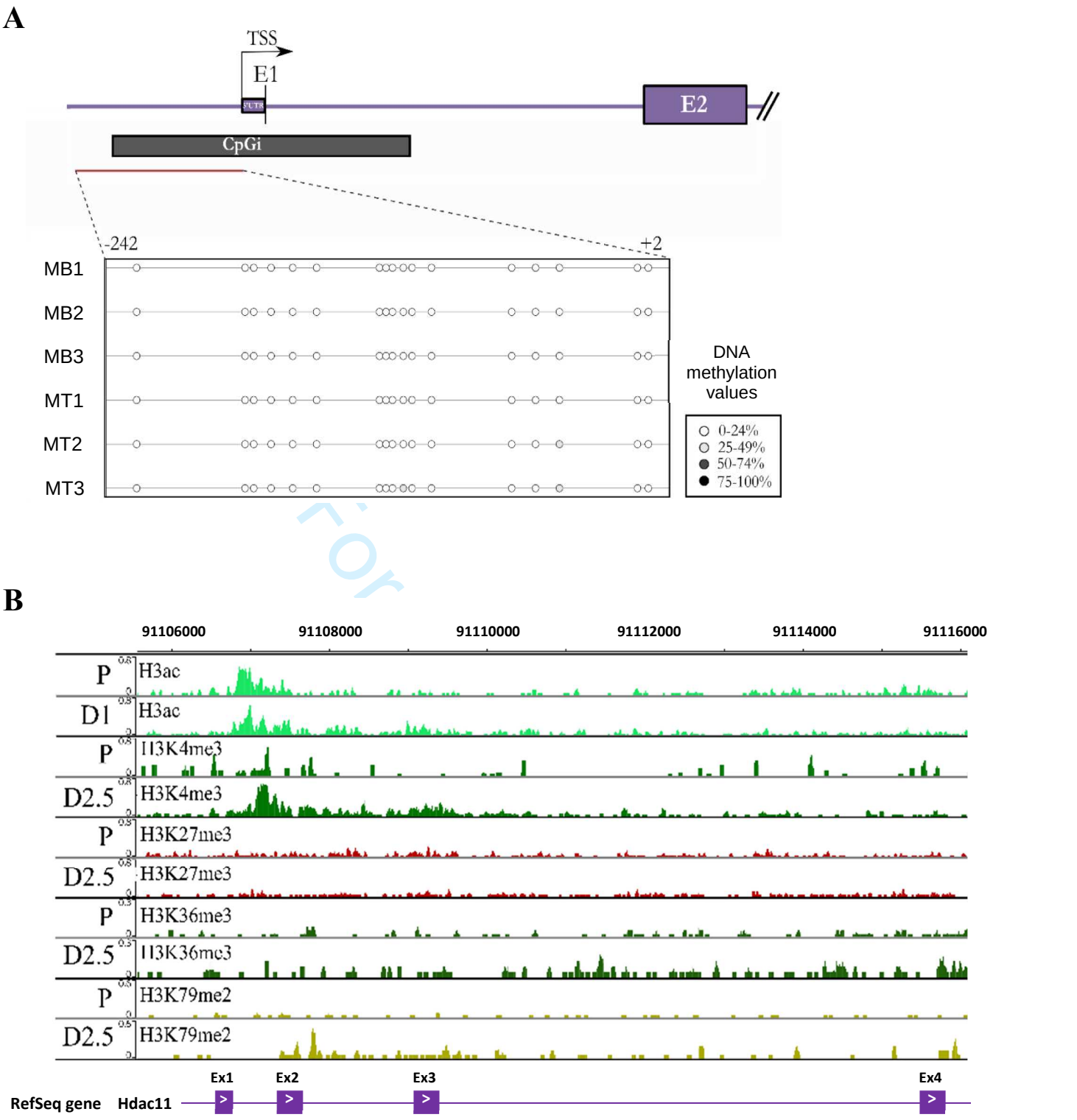

Supplemental Figure 2. Epigenetic landscape of *Hdac11* genomic locus.
A) Scheme of a partial region of *Hdac11* genomic locus and the corresponding analyzed region by DNA bisulfite sequencing (red line). The starting and end position of the analysed region is indicated relative to the TSS. The circles represent the cytosines of the CpG dinucleotides analyzed in three independent sets of satellite cell-derived primary myoblasts in proliferation (MB) and at 3 days of differentiation (MT), and the filling color represents the methylation level indicated in the legend. **B)** ENCODE bigwig tracks visualized with WashU Epigenome Browser of the indicated histone modification marks in a partial region of Hdac11 genomic locus (bottom) in proliferating (P) and 2.5 days differentiated (D2.5) C2C12 cells.

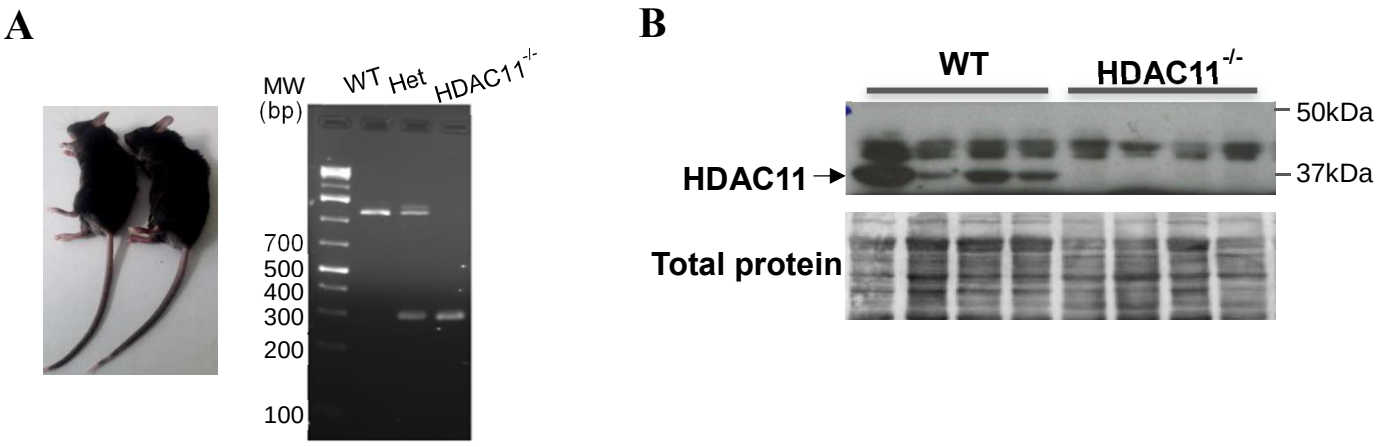

Supplemental Figure 3. Validation of HDAC11 knockout mice.

A) Image comparing WT and HDAC11$^{-/-}$ three-month old mice and confirmation by PCR of WT (+/+), heterozygote (+/-) and HDAC11 knockout (-/-) genotypes. **B)** WB analysis of HDAC11 expression from WT and HDAC11$^{-/-}$ brain samples. Total protein staining was used as a loading control.

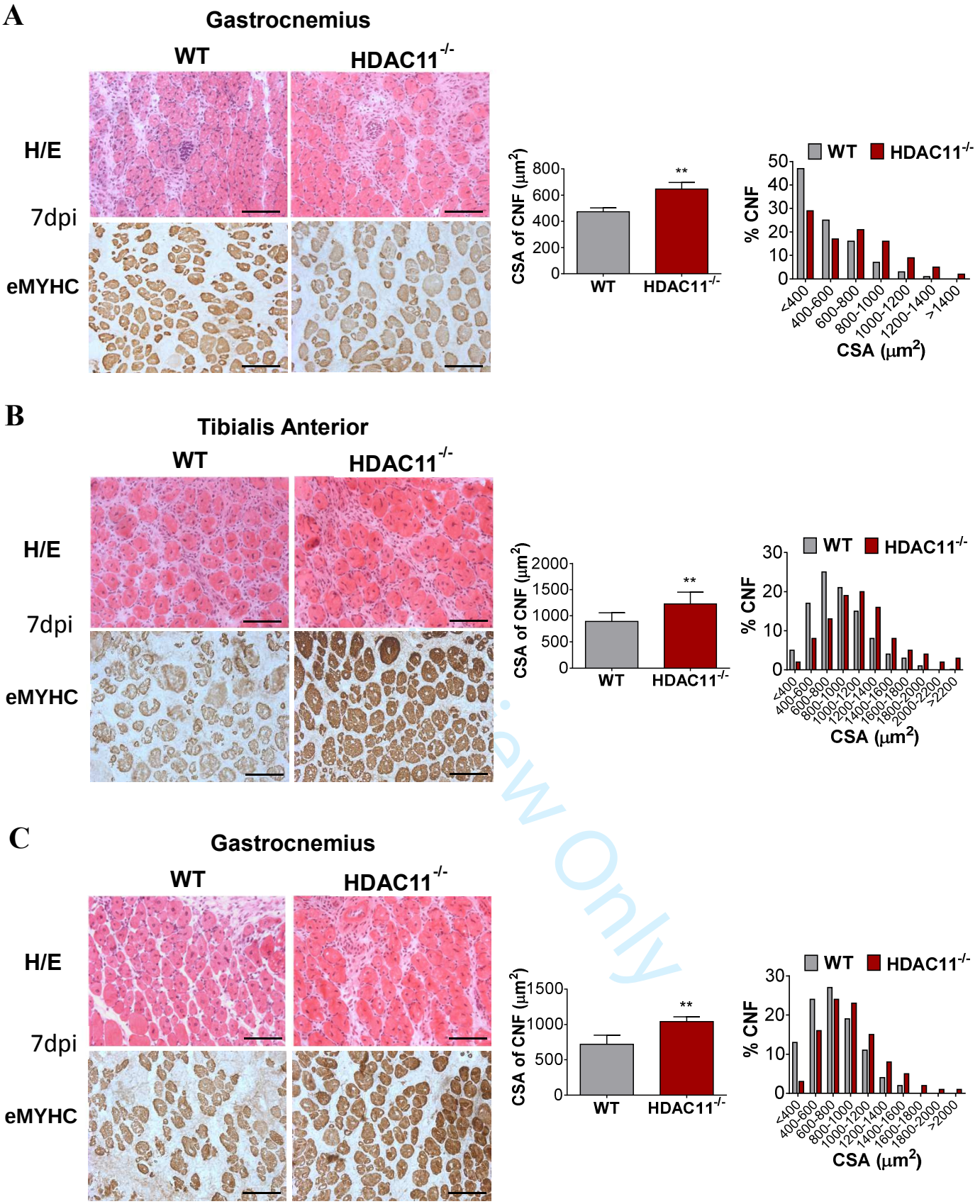

Supplemental Figure 4. HDAC11-deficient female mice show accelerated muscle regeneration at 7 days post-injury. A) Left: Hematoxylin/eosin (H/E) and embryonic myosin (eMYHC) staining of representative sections of gastrocnemius (GC) muscles from WT and HDAC11$^{-/-}$ male mice at 7 days post- injury. Scale bar: 100 µm. Right: Average cross-sectional area (CSA) of the central-nucleated regenerating fibers (CNFs) at 7dpi, and regenerating fiber size distribution represented as percentage of CNFs in the indicated area intervals. **B-C)** Same representation as in A, but analysing female mice in tibialis anterior muscles (B) and gastrocnemius muscle (C). Data information: n = 3-5 mice of 3 months of age for each group. A minimum of 300 CNFs were analyzed per muscle and animal using at least 5 random images per animal. Data are represented as means ± SD. Statistical significance was determined by unpaired t-test with two tails for CSA data and by ANOVA test for distribution of CNFs; **: p val <0.01.

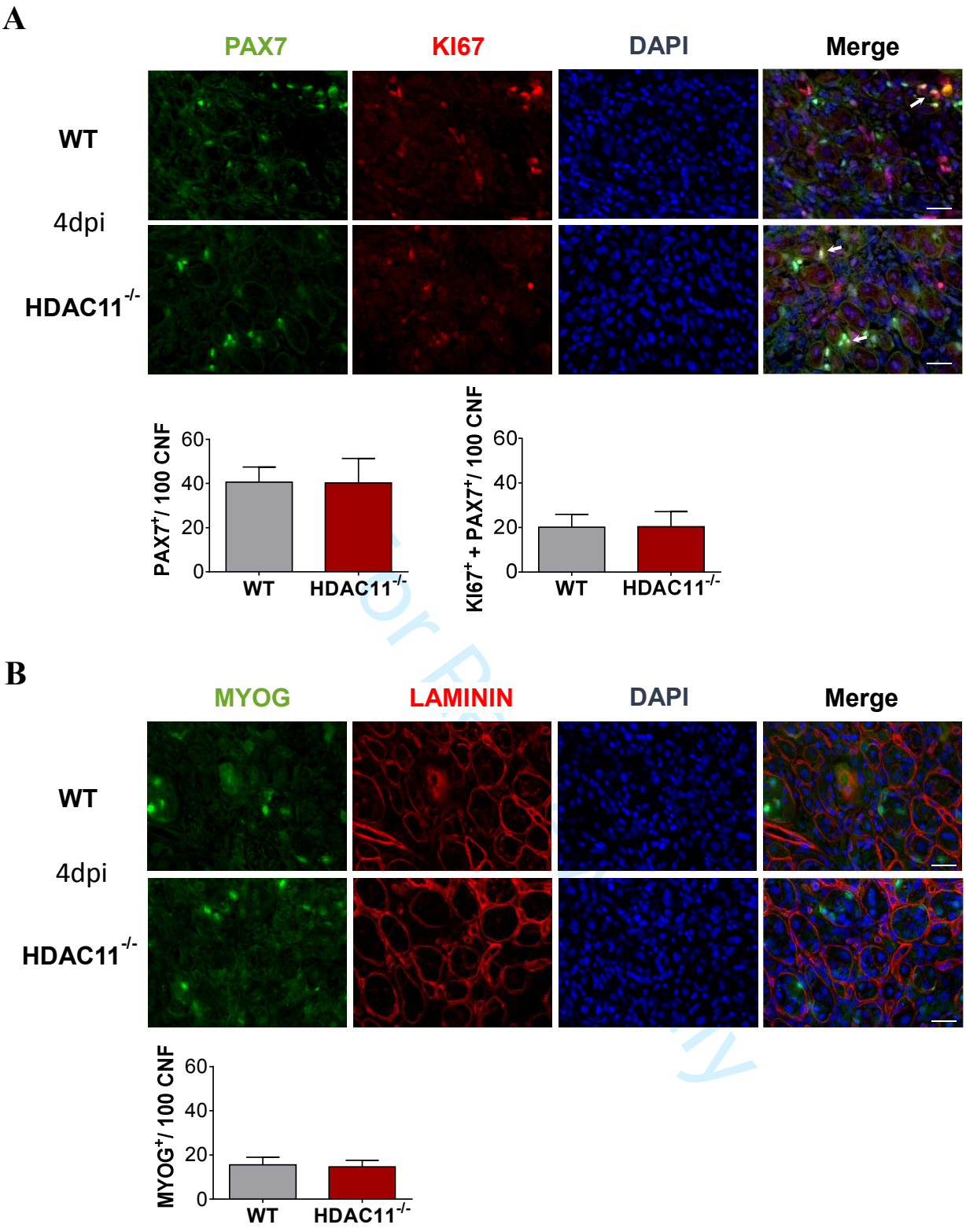

Supplemental Figure 5. HDAC11$^{-/-}$ mice do not show differences in satellite cells proliferation or differentiation at 4dpi.

A) Top: Representative sections of tibialis anterior muscles from WT and HDAC11$^{-/-}$ mice at 4dpi stained with PAX7 (green), KI67 (red) and DAPI (blue). Arrows indicate SCs that are PAX7^{+}/KI67^{+}/DAPI^{+}. Scale bar: 25 µm. Bottom: Quantification of PAX7^{+} SCs and PAX7^{+}/KI67^{+} SCs number per 100 CNFs. **B)** Top: Representative sections of tibialis anterior muscles from WT and HDAC11$^{-/-}$ mice at 4dpi stained with MYOG (green), LAMININ (red) and DAPI (blue). Scale bar: 25 µm. Bottom: MYOG^{+} SCs number per 100 CNFs. Data information: n = 3-4 male mice of three months of age for each group. A minimum of 300 CNFs were analysed per muscle and animal using at least 5 random images per animal. Data are represented as means ± SD and statistical significance was determined by unpaired t-test with two tails.

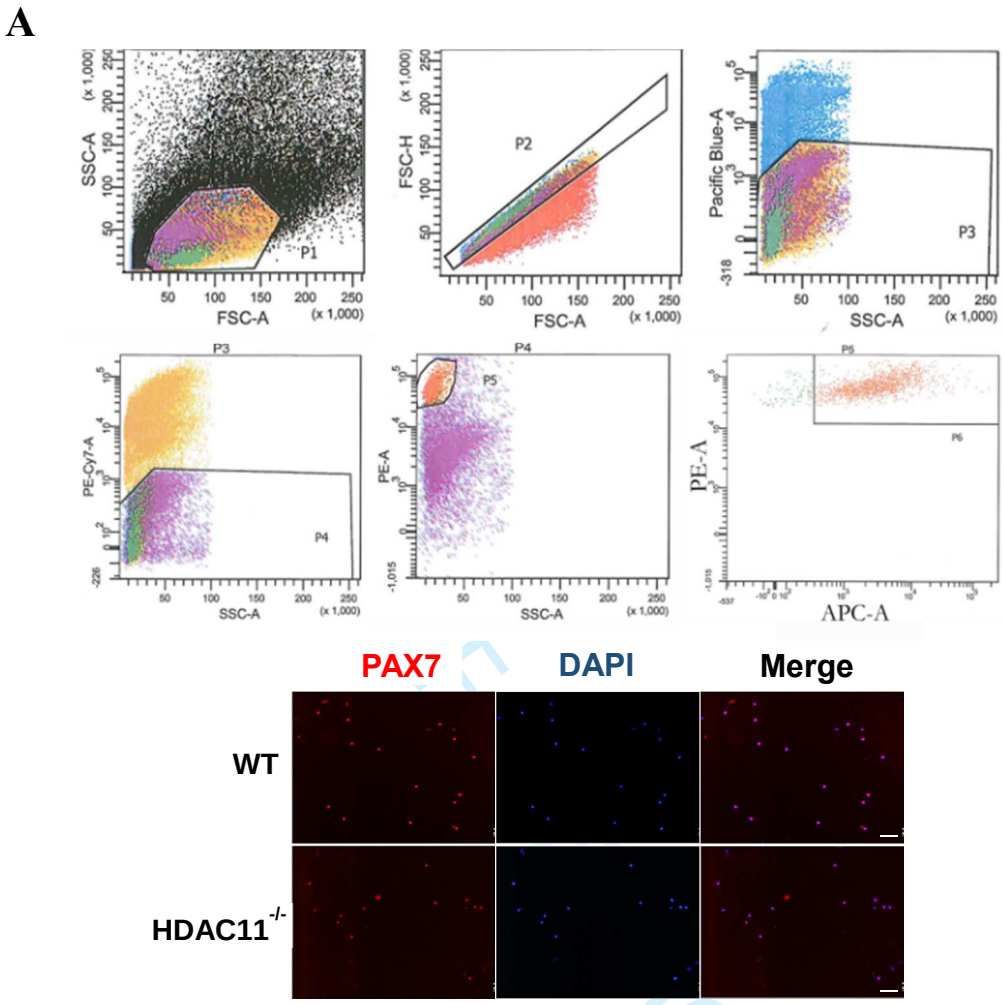

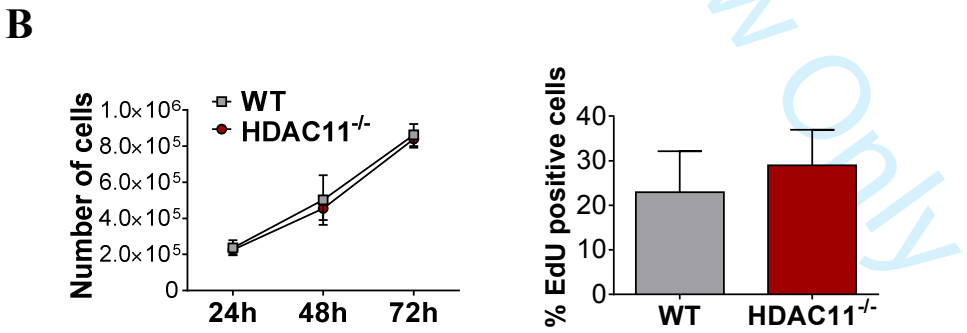

Supplemental Figure 6. HDAC11-deficiency does not alter myoblasts proliferation capacity of muscle primary cell cultures.

A) Top: Representative FACS plots and gating schemes to isolate mononucleated satellite cells (SCs) from heterogeneous populations of muscle extracts as described in [54]. Bottom: representative images of immunofluorescences with PAX7 staining in freshly isolated WT and HDAC11$^{-/-}$ satellite cells by FAC sorting. Almost 100% of isolated SCs were positive for PAX7 staining. **B)** Left: Growth curves of three independent sets of WT and HDAC11$^{-/-}$ satellite cell-derived primary myoblasts. 200,000 cells for each condition were seeded in 100 mm plates and counted each 24h. Values represent the average value of counts at each time point ± SD. Right: Percentage of stained EdU cells by FACS analysis in proliferating WT and HDAC11$^{-/-}$ satellite cell-derived primary myoblasts. Data represents the average values of three independent experiments ± SD. Statistical significance was determined by paired t-test with two tails; *: p val <0.05.

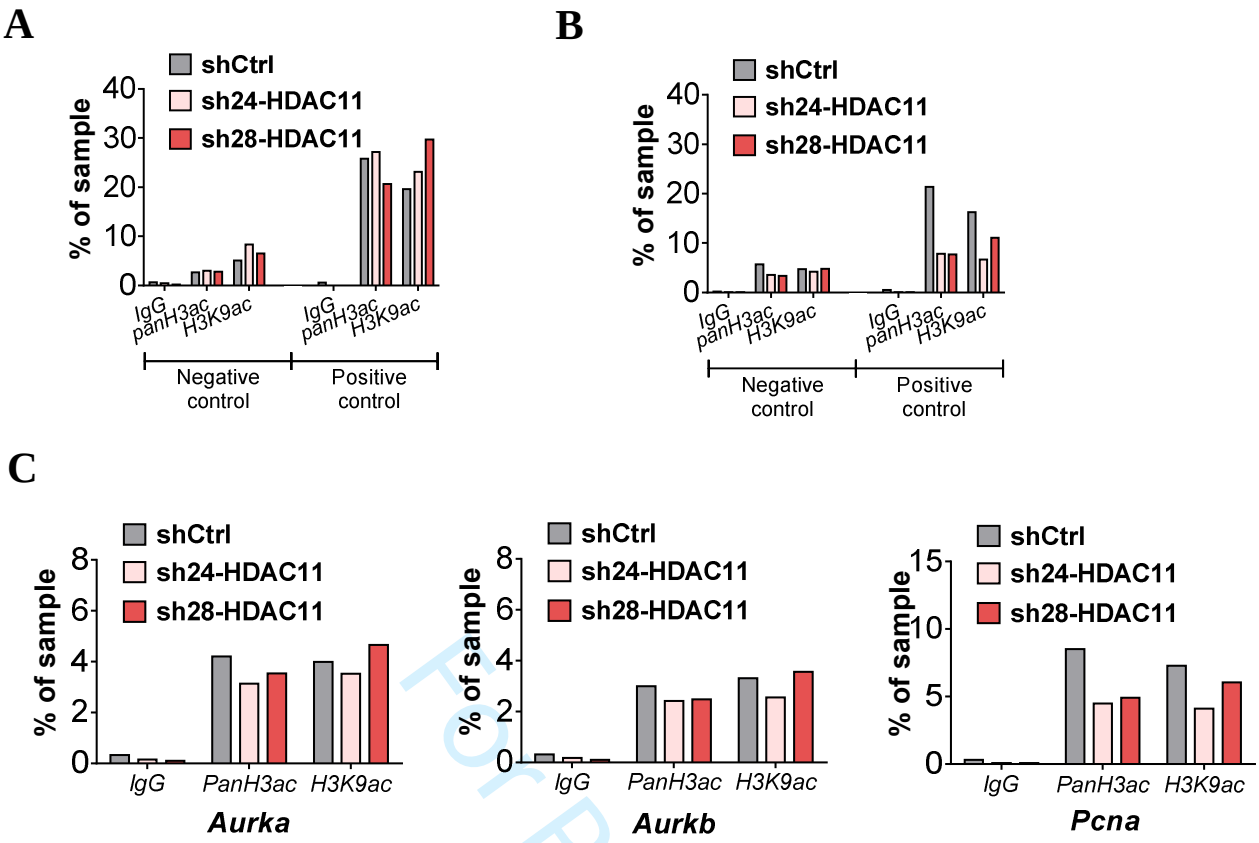

Supplemental Figure 7. HDAC11$^{-/-}$ differentiating myoblasts do not show different histone acetylation levels in promoter regions of cell-cycle related genes.

A-B) Representative experiment of histone marks enrichment assessed by ChIP-qPCR analysis, in the same samples than in Figure 6E, in a gene desert of chromosome 6 as a negative control region and in the promoter of ACTB1 gene as a positive control region. The results were normalized by input in A and by total H3 levels in B. **C)** Representative experiment of histone marks enrichment assessed by ChIP-qPCR analysis in the same samples than in Figure 6E normalized by total H3 levels.

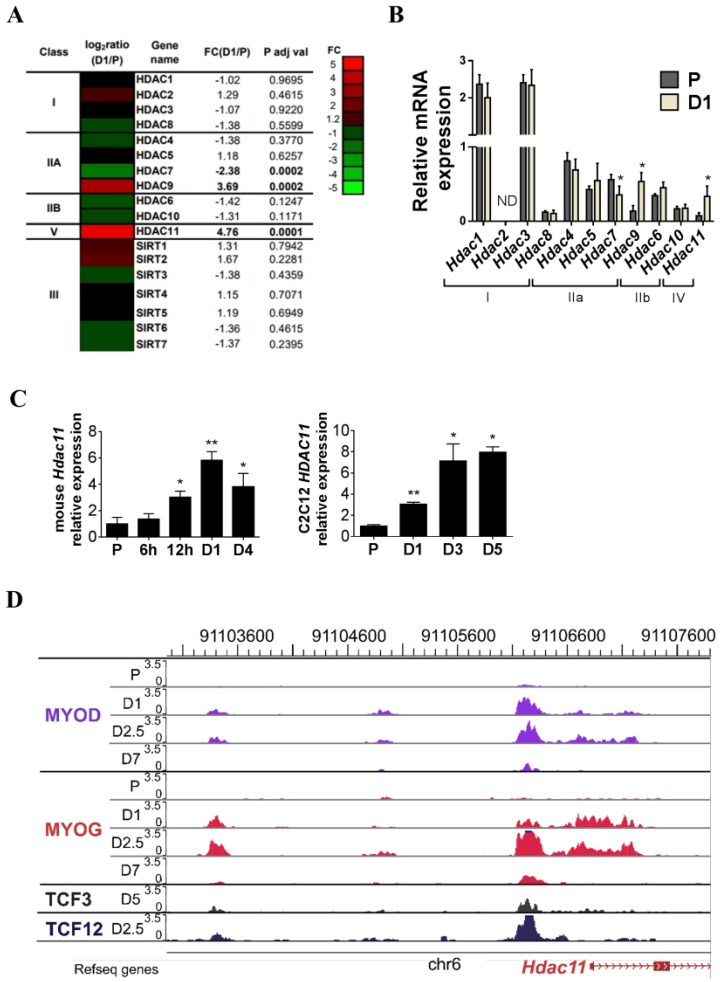

Figure 1, Núñez-Álvarez et al

Figure 1. HDAC11 is the HDAC member with maximal gene-expression induction at the onset of satellite-cell differentiation

A) Microarray data showing expression fold change (FC) of all HDAC family members between day 1 differentiating (D1) and proliferating (P) satellite-cell-derived primary myoblasts. B) Microarray validation by RT-qPCR of classical HDACs in differentiating (D1) and proliferating (P) satellite-cell-derived primary myoblasts. C) Expression level of HDAC11, by RT-PCR, in differentiation time-courses in mouse and human satellite-cell-derived primary myoblasts (left and middle grafts, respectively), and in C2C12 cell line (right graft). Data represent the average of four independent sets of satellite cell-derived primary myoblasts for mouse samples and two for human samples ± SD. ND means not detected. Three independent technical replicates were performed for C2C12 cells. Paired t-test with two tails was applied to assess statistical significance. *: p val <0.05; **: p val < 0.01. D) ENCODE ChIP-seq bigwig tracks of MYOD, MYOG and E-proteins TCF3 and TCF12 at proliferation and differentiation points. Data visualized using WashU Epigenome Browser browser v40.6 mm9.

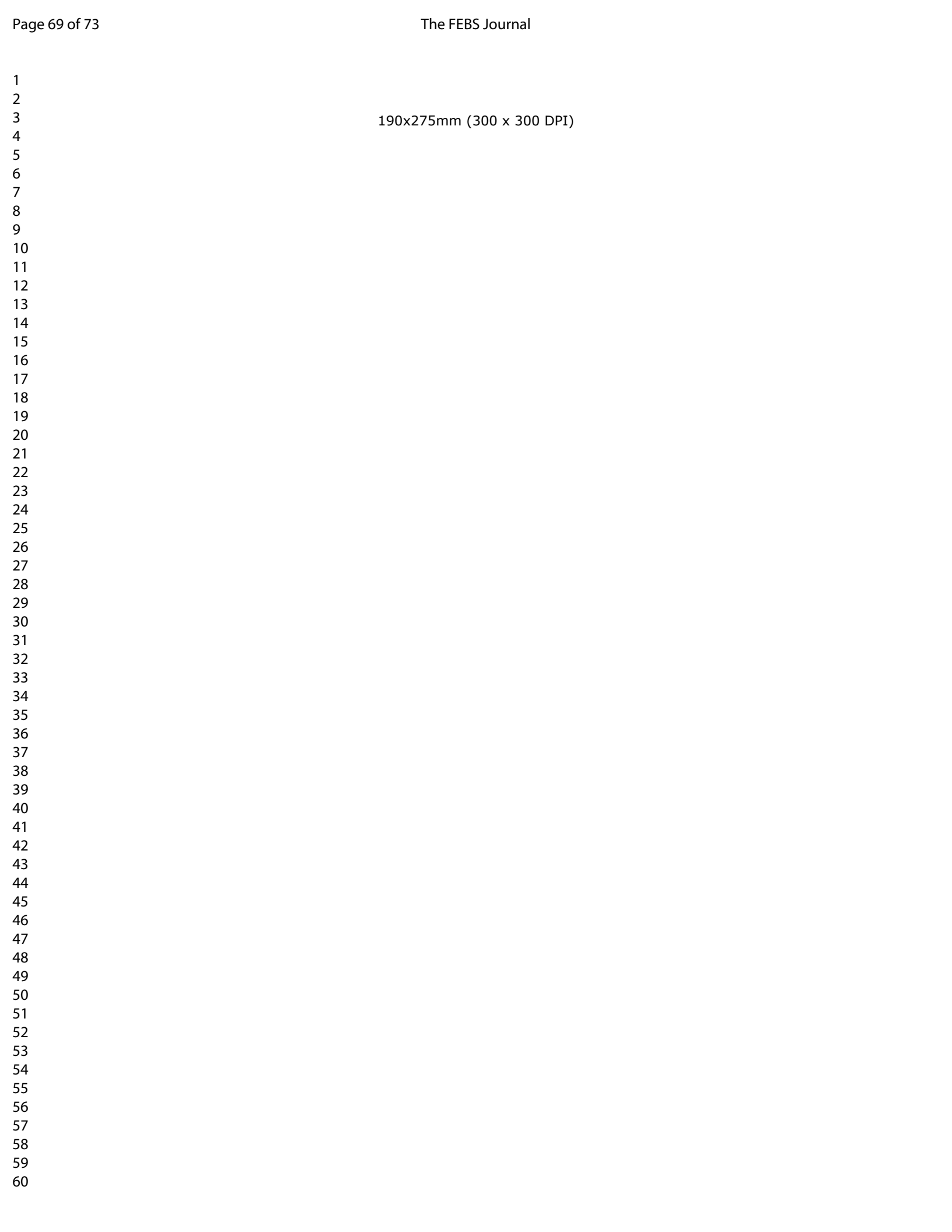
190x275mm (300 x 300 DPI)

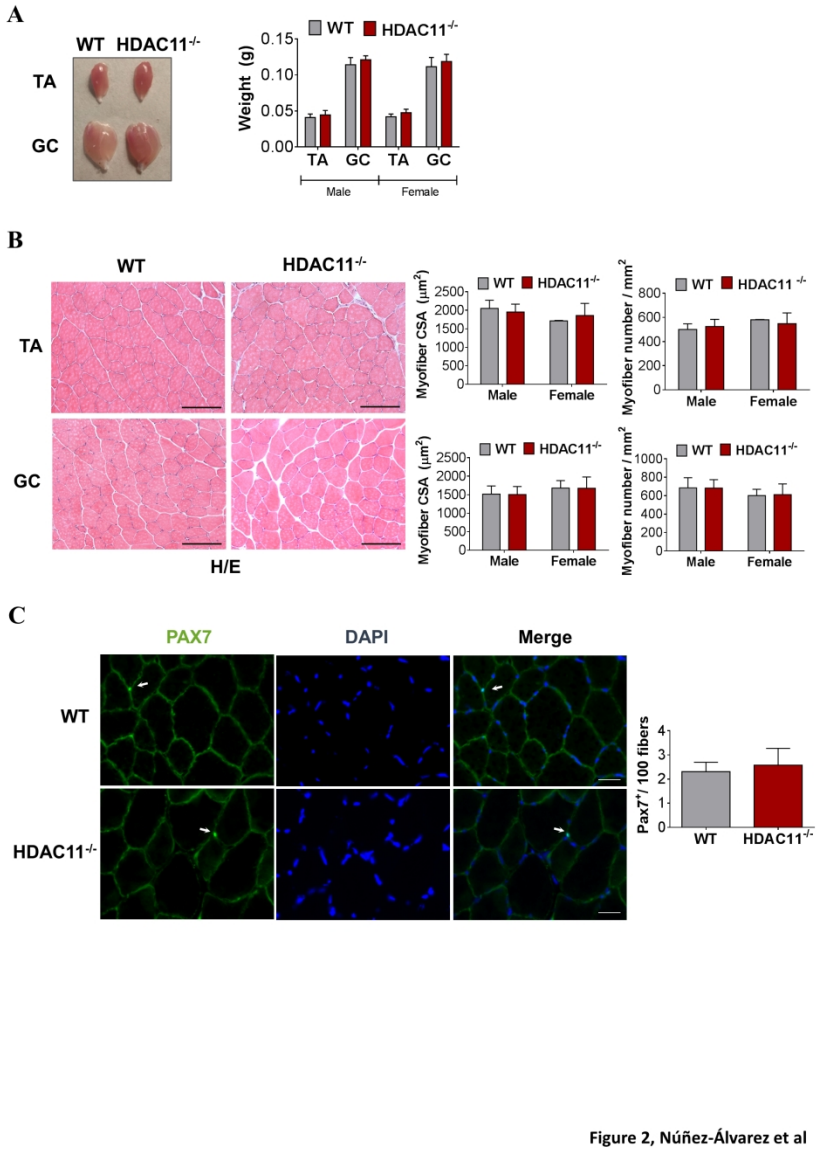

Figure 2, Núñez-Álvarez et al

Figure 2. HDAC11 is dispensable for adult skeletal muscle growth and homeostasis
A) Left: Representative image of a tibialis (TA) and gastrocnemius (GC) muscles from HDAC11 wild-type (WT) and knock-out (HDAC11-/-) mice. Right: Average weight in grams of TA and GC muscles ± SD. B) Left: Hematoxylin/eosin (H/E) representative sections of TA and GC muscles from WT and HDAC11-/- mice. Right: Average values of male and female myofiber cross-sectional areas (CSA) and number of myofibers/mm2. Scale bar: 100 µm. C) Left: Representative sections of TA muscles from WT and HDAC11-/- mice stained with PAX7 (green) and DAPI (blue). Arrows indicate SCs that are PAX7+/DAPI+. Right: Quantification of PAX7+ SC number per 100 fibers. Scale bar: 25 µm. Data information: n = 4-6 mice of three months of age for each group. In (B) and (C) a minimum of 400 myofibers were analysed per muscle and animal. Data are represented as means ± SD and statistical significance was determined by unpaired t-test with two tails.

190x275mm (300 x 300 DPI)

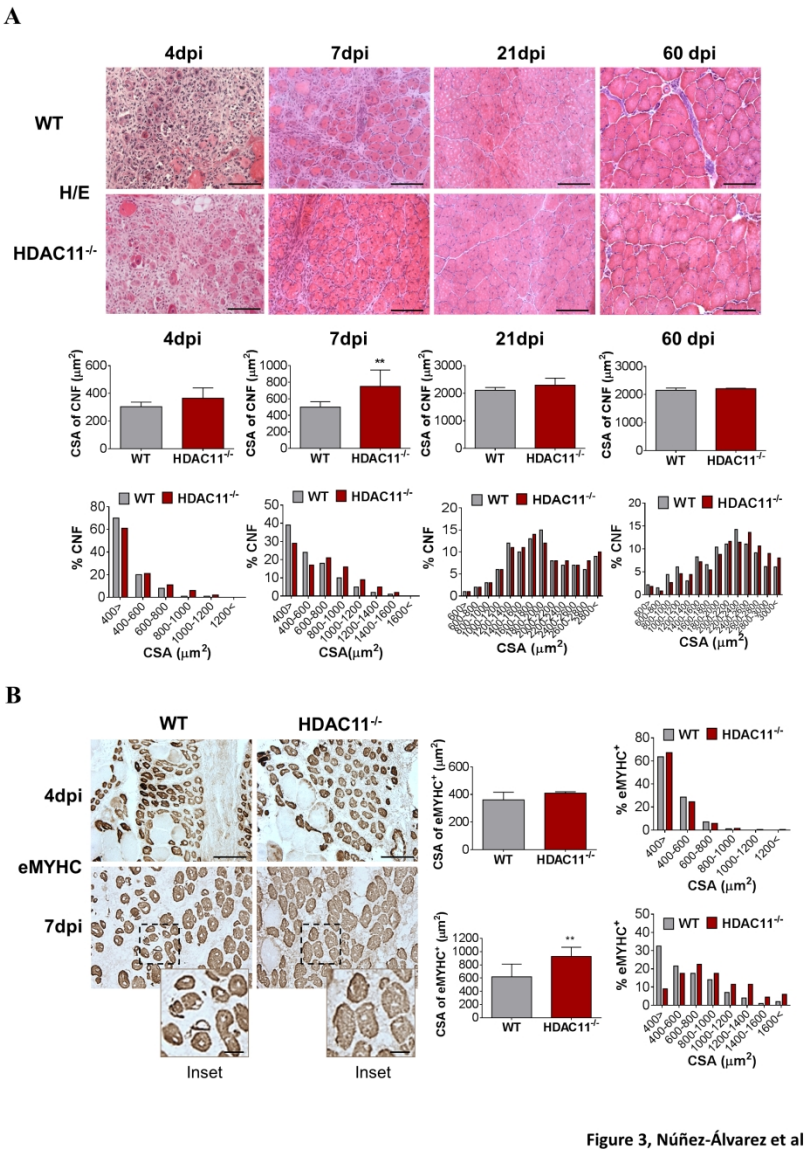

Figure 3. Skeletal muscle regeneration is accelerated in HDAC11-deficient mice

A) Top: Hematoxylin/eosin (H/E) representative sections of tibialis anterior (TA) muscles from WT and HDAC11-/- male mice at the indicated points after injury. Scale bar: 100 µm. Bottom: Average cross-sectional area (CSA) of the central-nucleated regenerating fibers (CNFs) at the same time points after injury, and regenerating fiber size distribution represented as percentage of CNFs in the indicated area intervals. B) Left: Representative sections of TA male muscles stained with embryonic myosin heavy chain (eMYHC) to visualize regenerating fibers at 4 and 7 days post injury. Scale bar: 100 µm. Inset: 25 µm. Right: Average cross-sectional area (CSA) of eMYHC-positive myofibers at the same time points after injury, and regenerating fiber size distribution represented as percentage of eMYHC+ myofibers in the indicated area intervals. Data information: n = 3-5 mice of 3 months of age for each group. A minimum of 300 CNFs were analysed per muscle and animal using at least 5 random images per animal. Data are represented as means ± SD. Statistical significance was determined by unpaired t-test with two tails for CSA data and by two-way ANOVA test for distribution of CNFs; **: p val <0.01.

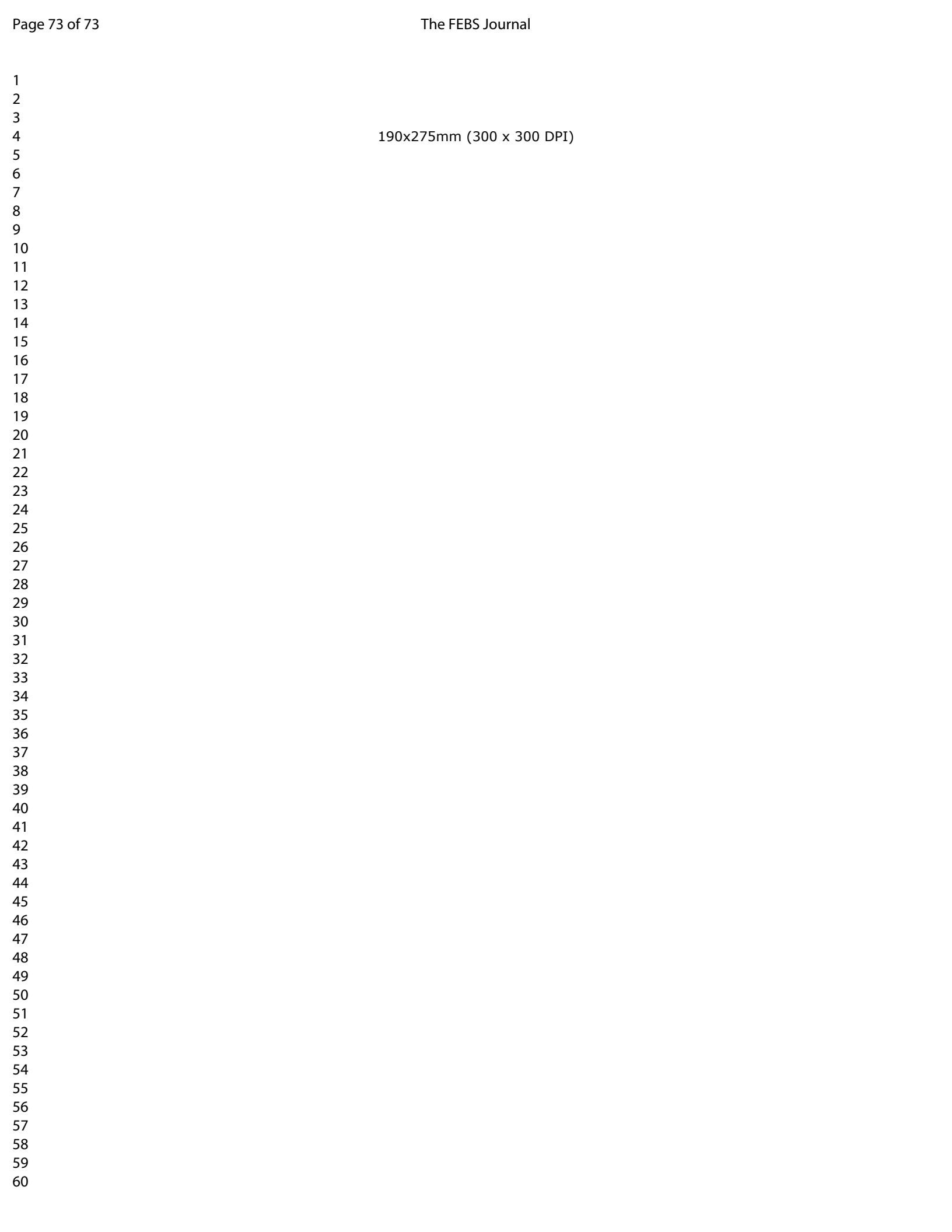
190x275mm (300 x 300 DPI)

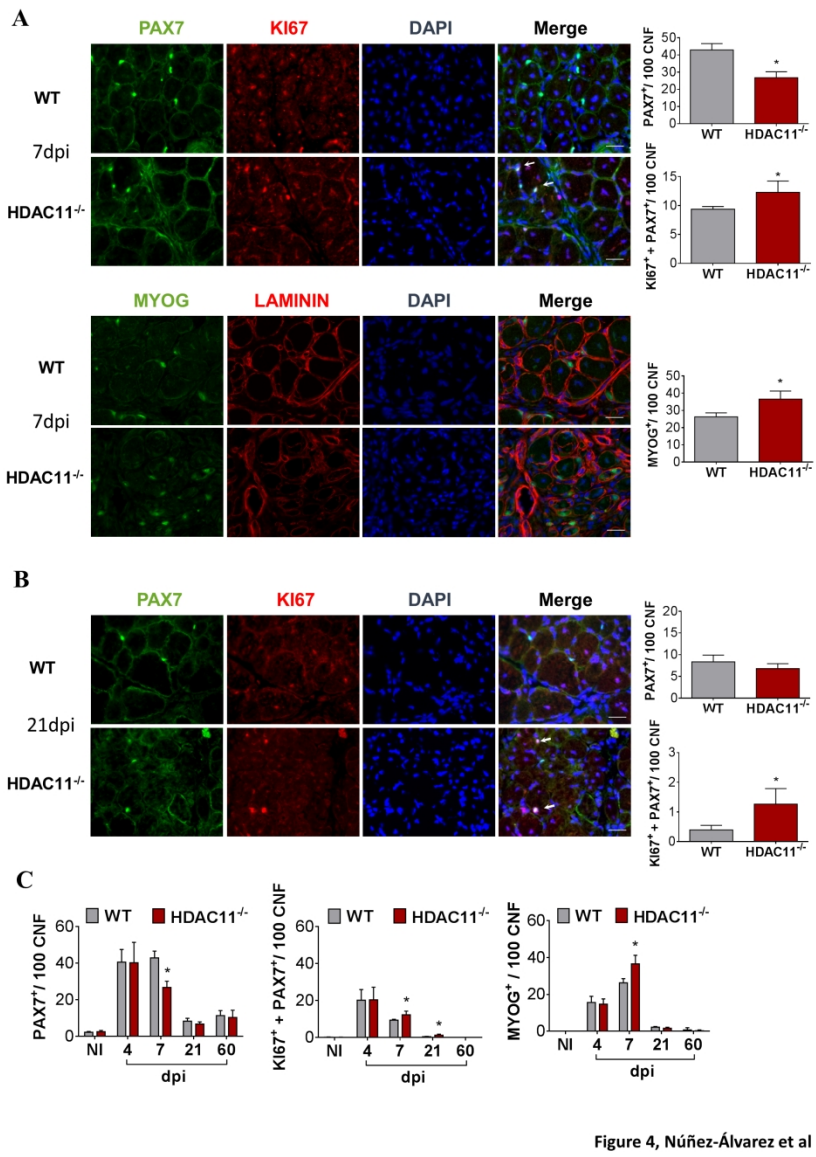

Figure 4. HDAC11 deficiency alters satellite-cell differentiation kinetics during skeletal muscle regeneration

A-B) Left: Representative sections of tibialis anterior muscles from WT and HDAC11-/- mice at 7dpi (A) and 21dpi (B). Muscles were stained with PAX7 (green), KI67 (red) and DAPI (blue) or MYOG (green), LAMININ (red) and DAPI (blue). Arrows indicate SCs that are PAX7+/KI67+/DAPI+. Scale bar: 25 μm. Right: Quantification of PAX7+ SCs number, PAX7+/KI67+ SCs number and MYOG+ SCs number per 100 CNFs. C) Quantification of PAX7+ SCs number, PAX7+/KI67+ SCs number and MYOG+ SCs number per 100 CNFs in not injured (NI), 4, 7, 21 and 60 days post injured WT and HDAC11-/- muscles. Data information: n = 3-6 male mice of three month of age for each group. A minimum of 300 CNFs were analysed per muscle and animal. Data are represented as means ± SD and statistical significance was determined by unpaired t-test with two tails. *: p val <0.05.

190x275mm (300 x 300 DPI)

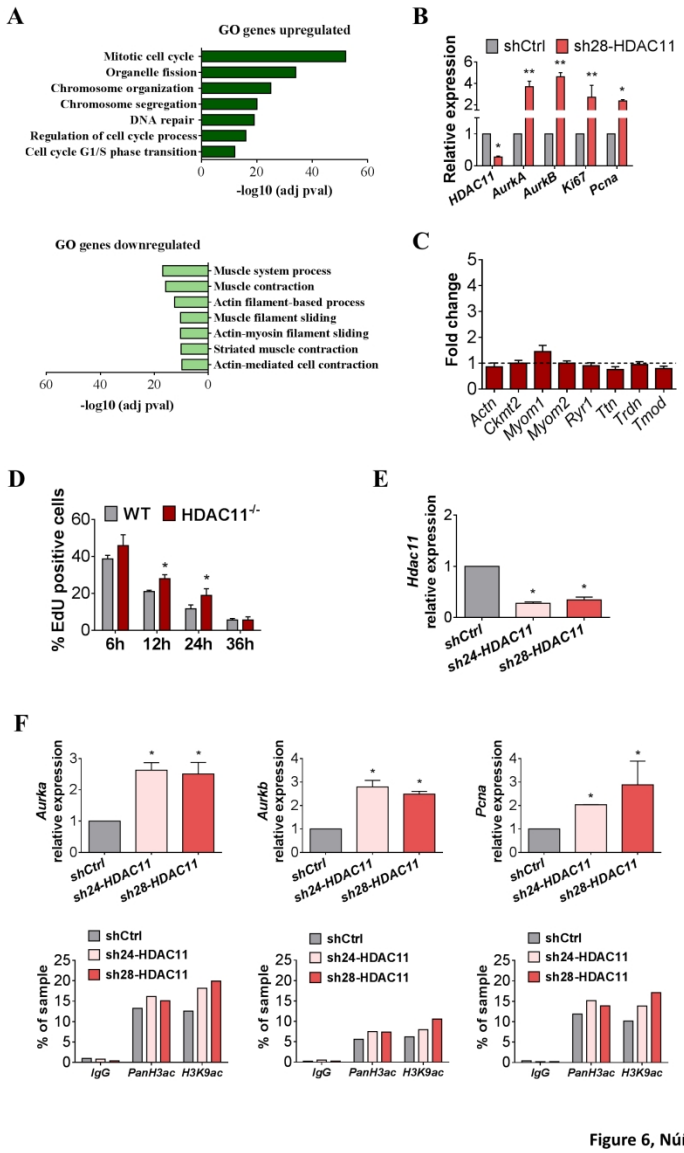

Figure 6, Núñez-Álvarez et al

Figure 6. HDAC11-/- myoblasts express higher levels of cell cycle-related genes and exhibit sustained proliferation in differentiating conditions

A) Graphical representation of the 7 top statistically significant gene ontology (GO) terms enriched in gens overexpressed (dark green bars) or downregulated (light green bars) in HDAC11-/- day 1 differentiating myoblasts compared to WT counterparts. B) Independent RT-qPCR validation of selected genes (identified as upregulated by RNA-seq in mouse HDAC11-/- myocytes) in C2C12 cell lines expressing non-mammalian targeting (shCtr) and HDAC11 targeting shRNAs. Data show HDAC11 depletion and upregulation of the indicated targets measured in three independent experiments ± SD. C) Quantification of mRNA levels by RT-qPCR of different sarcomere-related genes and calcium sensing/releasing-related genes in TA muscles from WT and HDAC11-/- three-month old mice. WT expression reference value = 1. D) FACS quantification of the proportion of EdU stained cells at 6, 12 and 36 hours after induction cell differentiation in WT and HDAC11-/- satellite cell-derived primary myoblasts. Data represents the average values of three independent experiments ± SD. E) Quantification of expression level by RT-qPCR of HDAC11 in C2C12 cell lines expressing non-mammalian targeting (shCtr) and HDAC11 targeting shRNAs at 1 day of differentiation. On

the same cells, the expression level of Aurka, Aurkb and Pcna genes was determined by RT-qPCR before performing ChIP assays. Data represents the average of three independent experiments ± SD. Paired and unpaired t-test with two tails was applied to assess statistical significance between groups. *: p val <0.05. For each gene (Aurka, Aurkb and Pcna) a representative experiment of ChIP qPCR analysis for PanH3ac and H3K9ac, in the corresponding promoter regions, is shown. ChIP data were normalized to the corresponding input values.

190x275mm (300 x 300 DPI)

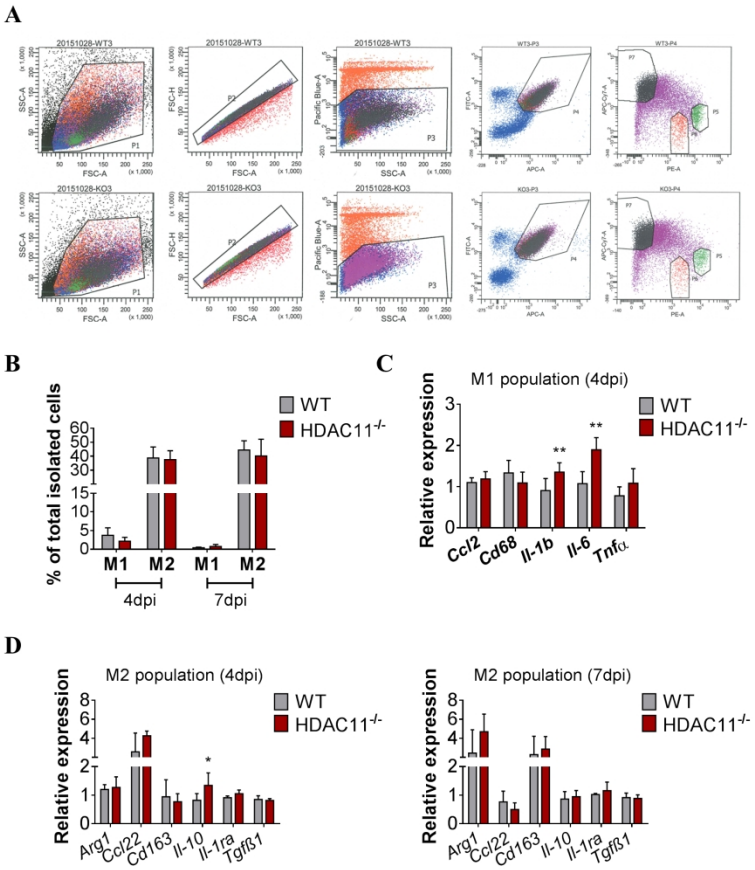

Figure 7, Núñez-Álvarez et al

Figure 7. HDAC11-deficient macrophages overexpress IL-10.
A) Representative FACS plots and gating schemes to isolate macrophages populations of muscle extracts as described in [58]. B) Percentage of total isolated macrophage subpopulations M1 and M2 from WT and HDAC11-/- muscles extracts at 4 and 7 days post injury (dpi). C) Quantification of expression levels of indicated cytokines by RT-qPCR from M1 isolated macrophages at 4 dpi. D) Quantification of expression levels of indicated cytokines by RT-qPCR from M2 isolated macrophages at 4 and 7 dpi. Data information: n = 4 male mice of three old age for each group. Data are represented as means ± SD and statistical significance was determined by unpaired t-test with two tails. *: p val <0.05; **: p val <0.01.

190x275mm (300 x 300 DPI)